Observations with the Li-Beam Diagnostic on W7-AS

S. Zoletnik, G.Kocsis, S. Fiedler, K. McCormick,
J. Schweinzer, W7-AS Team and HP. Winter

IPP III/213 August 1996

MAX-PLANCK-INSTITUT FÜR PLASMAPHYSIK

85748 GARCHING BEI MÜNCHEN

MAX - PLANCK - INSTITUT FÜR PLASMAPHYSIK
GARCHING BEI MÜNCHEN

Observations with the Li-Beam Diagnostic on W7-AS

S. Zoletnik, G.Kocsis, S. Fiedler, K. McCormick,
J. Schweinzer, W7-AS Team and HP. Winter

IPP III/213 August 1996

Die nachstehende Arbeit wurde im Rahmen des Vertrages zwischen dem Max Planck Institut für Plasmaphysik und der Europäischen Atomgemeinschaft über die Zusammenarbeit auf dem Gebiet der Plasmaphysik durchgeführt.

Observations with the Li-beam diagnostic on W7-AS

S. Zoletnik[1], G. Kocsis[1], S. Fiedler[2,3], K. McCormick[2]
J. Schweinzer[2] and HP. Winter[3]

[1] KFKI–Research Institute for Particle and Nuclear Physics, P.O.Box 49, 1525 Budapest-114, H-1525 HUNGARY

[2] Max-Planck-Inst. für Plasmaphysik, EURATOM Association, D-85748 Garching, GERMANY

[3] Institut für Allg. Physik, TU Wien, Wiedner Hauptstr. 8-10/134, A-1040 Wien, AUSTRIA

August 12, 1996

Abstract The aim of this report is to summarize some selected results obtained with the high energy Li-beam diagnostic at W7-AS. After exploring the capabilities and limitations of this diagnostic three topics are discussed: H-mode related phenomena, behaviour of the electron density profile at different rotational transform and electron density fluctuations.

1 Some details about the Li-beam diagnostic

For correct interpretation of the results it is necessary to understand the capabilities both of the measurement and data evaluation. It is assumed that the reader has a basic knowledge of the idea and operation of the Li-beam diagnostic.

The high energy Li-beam diagnostic[2, 3] on W7-AS [1] is located at $-18°$ toroidal angle in module 2. Fig.1 shows the position of the beam and its optical detection channels. The beam energy can be adjusted from 20 keV to 66 keV, but during the experiments in question it was fixed at 48 keV.

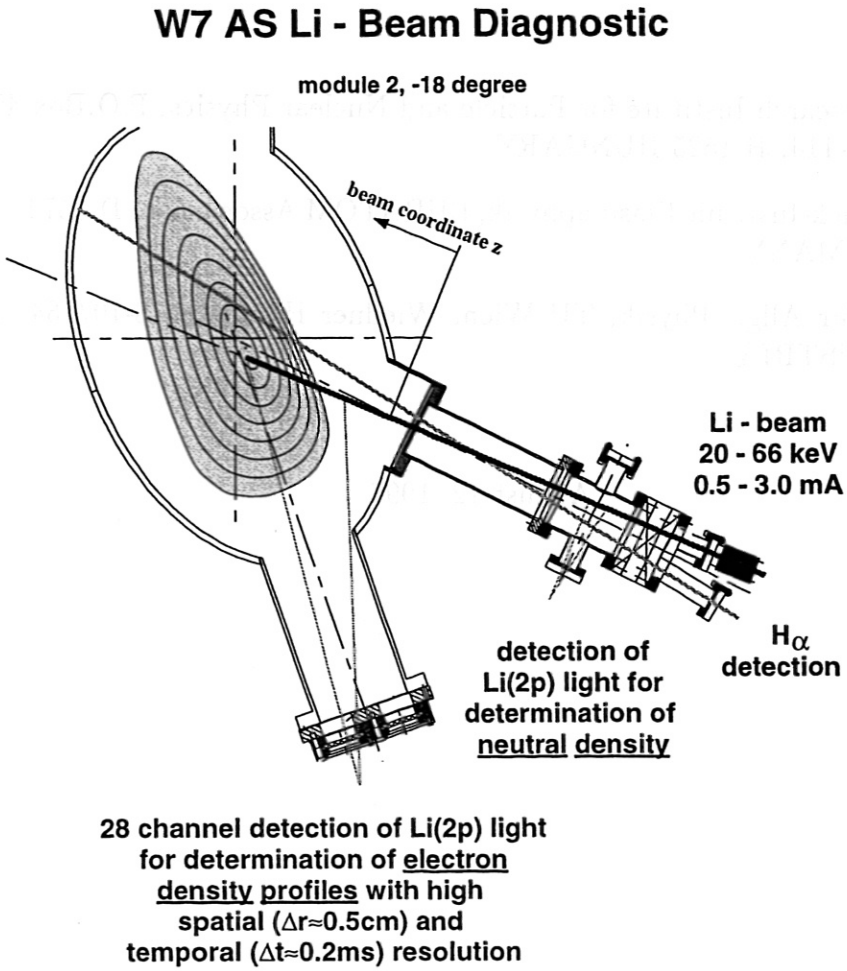

Figure 1: The Li-beam and its detection system

The light (Li 2p-2s transitions) of the beam in the plasma is detected by a 28 channel photomultiplier system. Spatial separation of these channels changes from 0.6 cm in the scrape-off layer to about 1 cm in the core plasma. The neutral Lithium atoms emit light due to excitations by collisions both with neutral and

charged particles in the plasma or gas. Using this fact, the detection channels were relatively calibrated after each plasma discharge individually, by applying a gas pulse in the W7-AS chamber after the shot and detecting the Li 2p light of the beam during this time period. The gas density is homogeneous in the vacuum chamber and the Li-beam is not attenuated within the observation region ($\approx 20cm$). Thus the Li 2p light intensity emitted by the beam atoms should be constant along the beam.

The light distribution is usually plotted as a function of distance along the beam, denoted by Z. The starting point of this coordinate system is approximately at the W7-AS vacuum vessel flange (see Fig. 1). The observation points are in the range of Z=10.4–29.5cm, thus smaller beam coordinates correspond to the plasma edge. In order to enable comparison with other diagnostics, the Li-beam beam coordinates (Z) are transformed to equilibrium flux surface coordinates (R_{eff}) calculated by the Kisslinger–Wobig (KW) equilibrium code (free boundary) [4].

As the detection system uses a relatively wide transmission band interference filter, the background (non Li 2p) light detected by the photomultipliers can be rather high. In low density shots it is typically in the 10 percent range (depending on the radial position), but in a high density regime or during NBI it can reach several hundred percent relative to the Li 2p light. One of the most critical factors of the data processing is therefore a good approximation of the background light level. As in most experiments it is not possible to have a background shot, the only way to get rid of this background signal is to chop the Li-beam and measure the background light level in regular intervals. In the experiments discussed here, a mechanical chopper was used, having a period time of approximately 60 ms, and a beam-off time of about 5 ms. In this way a good background subtraction can be done for phenomena with characteristic times much longer than 60 ms. On the other hand, short ($\leq 5ms$) periodic or nearly-periodic phenomena can also be analyzed by comparing events during the beam-off and beam-on times.

Besides the 28 Li-IXS (Impact Excitation Spectroscopy) channels two other light signals are detected. One called neutral density signal is related to the light emitted by the beam before entering the plasma. This light originates from the interaction of the Li beam atoms with the neutral gas in the W7-AS vessel port. If the neutral gas density in the port is constant in time the neutral density signal can be used as a Li-beam monitor. On the other side, if the Li-beam current is known (e.g. from the emitter current and the neutralization efficiency) the neutral density signal can be used to monitor the neutral gas density in the port during the plasma discharge.

Additionally, H_α light is collected by viewing approximately along the Li-beam axis and detected by an H_α filter/photomultiplier setup. As this signal proved to be a very good indicator of the L–H-mode transition, in the rest of this report the phrase "H_α signal" will refer to this signal and not to other measurements of H_α radiation at W7-AS (e.g. H_α observation at the limiters).

All of the above described 30 signals were electrically filtered by 0.2ms RC time constant passive integrators, and digitized at 5 kHz sampling rate.

For the construction of the Li 2p light profile from the raw signals three main error sources were identified. The most obvious one is photon statistical noise. This was estimated to be less than one percent for the channels with the least light (sides of the profile). The error of the calibration factors was investigated by analyzing their changes in a series of 24 shots. It was found that the average calibration error (RMS deviation of calibration factors) for the 28 Li-IXS channels is about one percent. The error resulting from the uncertaintity of the background light subtraction depends on the actual plasma condition, thus no general estimate can be given. (Low background light level in ECRH heated discharges, and high background in shots with additional neutral beam heating.)

The *absolute* electron density distribution along the Li-beam is unfolded from the *relative* light profiles by a five-atomic-level method [5], capable of taking into account both the electron temperature and the Z_{eff} profile of the plasma. However, it was shown previously [6], that the calculated electron density profile is not very sensitive to T_e and Z_{eff} changes. It should be noted, that even in the plasma edge, where Li-beam attenuation is negligible, the local Li 2p light signal is not determined only by local plasma parameters. The Li 2p level has a finite lifetime and thus the beam velocity produces an integration of the Li 2p light signal with an e-folding decay length of about 3 cm (at a beam energy of 48 keV). The density reconstruction program accounts for this effect.

Another limitation of the measurement is that the inaccuracy of the calculated electron density becomes large if the beam is substantially attenuated, see Fig 2 for $Z > 22cm$. To avoid problems, the density profiles used in this report were usually calculated only to the maximum of the Li 2p light signal.

As the calculated density at a given position along the beam is determined by the whole light profile, it is very difficult to give error bars for the reconstructed density profile. To get an impression about the error of the reconstructed density profile, one can perform several calculations using the same light profile with an added computer generated noise of appropriate amplitude. This added noise simulates both the inaccuracy of calibration factors and photon statistical noises. The average and standard deviation of the resulting density profiles can be calculated. An example of such a result is plotted in Fig. 2. As expected, the density calculation is uncritical up to the location, where the light profile has its maximum. This error estimate indicates, that deeper in the plasma the inaccuracy of the calculated density can be rather high.

In some experiments a plateau showed up in the gradient region of the reconstructed electron density profile. (See e.g. Section 3.) In order to investigate how such a plateau is reconstructed, numerical tests were done using a program which can generate a light profile from an input density profile. This program uses the same physical model and measurement geometry as the density deconvolution pro-

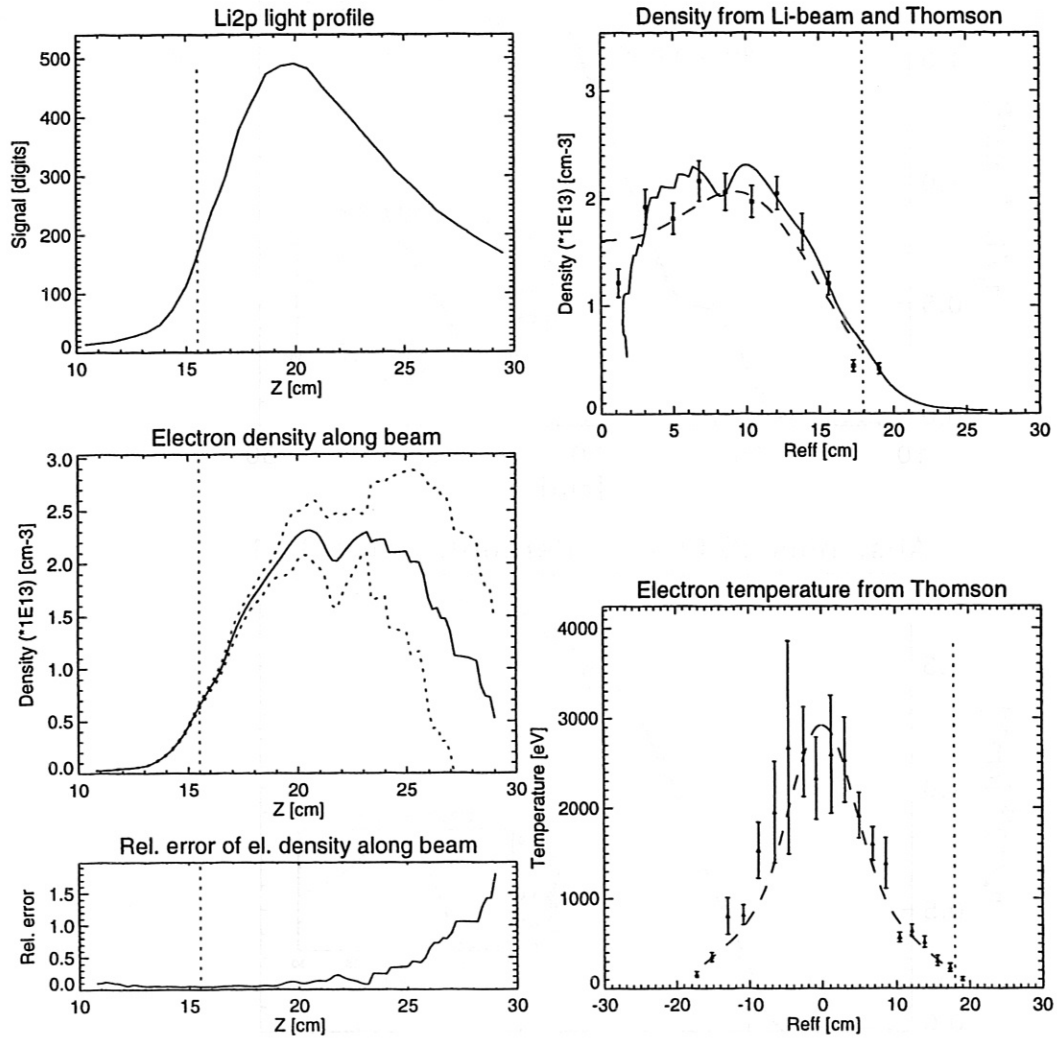

Figure 2: Li 2p light profile, reconstructed electron density and its error range both as a function of beam coordinate Z and flux surface coordinate R_{eff} (shot 27149, B_0=2.55T, ι_0 = 0.345, limiters at 31.5cm, time of measurement: 0.580 − 0.585s). The dashed vertical lines mark the position of the Last Closed Flux Surface (LCFS). Electron density values measured with Thomson-scattering (points with error bars) and fits to them (dashed lines) are shown for comparison. The Thomson electron temperature profile was used in the reconstuction process. See text for more details.

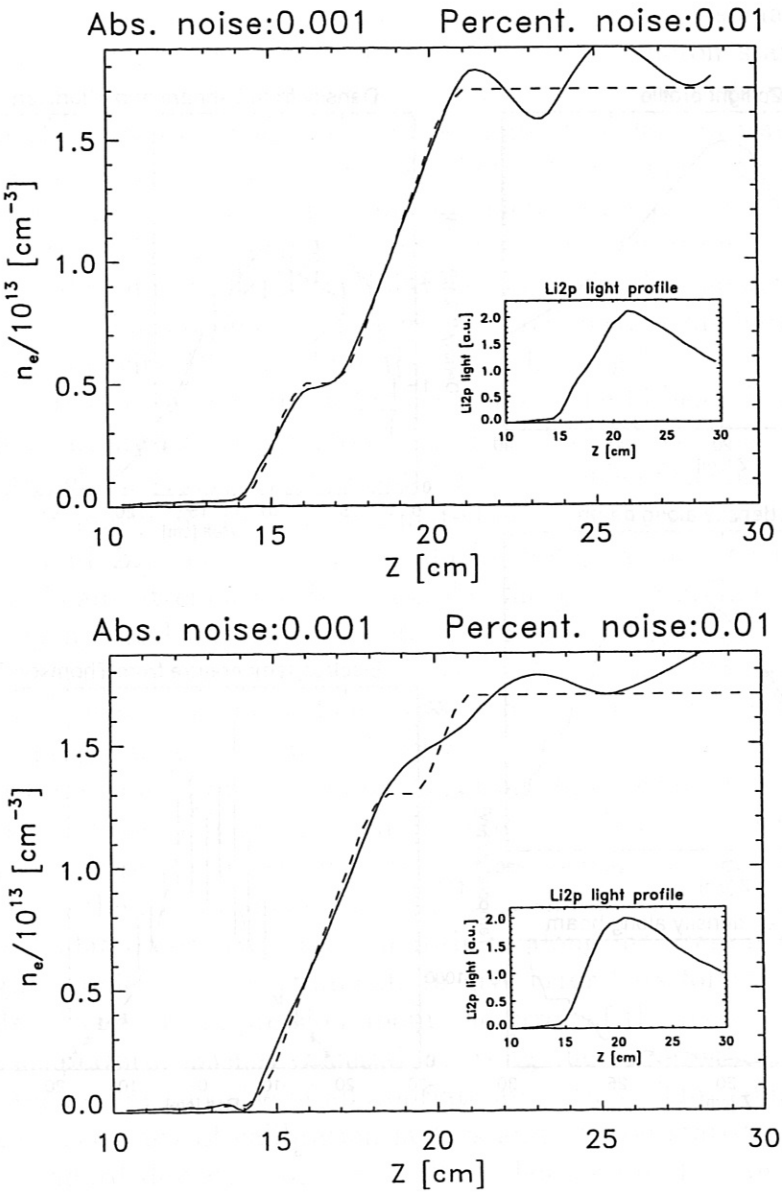

Figure 3: Reconstruction of electron density profiles from computer generated Li 2p light profiles. The solid line represents the reconstructed density profile, the dashed line the original density profile used as an input for the Li 2p light profile calculation. Computer generated white noise was added to the light profiles before reconstruction of the electron density profiles.

gram. Light profiles were calculated from prescribed density profiles with a 1 cm wide plateau in the gradient region. The location of the plateau was changed. Two examples are shown in Fig. 3. It was found, that a plateau in the density profile can be reconstructed if it is located in the rising part of the Li 2p light profile. Shifting the plateau close to the maximum of the Li 2p light profile, its reconstruction becomes doubtful as the method itself becomes unstable.

2 Results in H-mode experiments

Characteristic L–H-mode transitions were found in W7-AS [7] around $\iota \sim 0.5$, but H-mode like phenomena could be observed at other iota values too. As most phenomena associated with H-mode are accompanied with characteristic changes in the density profile at the plasma edge, the Li-beam diagnostic is well suited to investigate them.

It was found that during the H-mode experiments the most critical source of error is the estimation of the background light. Depending on the phenomena, different techniques were used to get a more or less reliable background light profile.

2.1 The L–H transition

A clear L–H transition could be observed in shots 28255-28277 and 28233-28236 (B_0=2.53T, ι=0.526), and 28700-28720 (B_0=2.48T, ι=0.509). As both, the point in time and the time evolution of the transition, differs from shot to shot, it is not possible to get a background light profile from a background shot (no Li-beam injection). As the characteristic time constant of the transition is about 5 ms, the chopper cannot be used to give a good background light estimate for the whole time evolution. In this way reliable density calculations could be performed only close to the chopper beam-off time intervals. A typical time evolution of the (background subtracted) Li 2p light profile and the H_α signal is shown in Fig. 4. The dips in the light profile are the chopper intervals.

As can be seen from this figure, the final transition at 0.3 s is preceded by several transient drops in the H_α signal. A closer look reveals a steepening of the Li 2p light profile at the edge, correlated with drops of the H_α signal. One might argue that this behaviour is caused by a change in the background light profile. This explanation is highly unlikely, as the steepened profile remains the same after the transition, even close to the next chopper time interval, where the background subtraction is correct. After the transition, a continuous increase of the Li-beam attenuation can be observed in the plasma core. This effect is in good agreement with the HCN interferometer measurement (see Fig. 5) indicating a continuous electron density increase after the transition. It can also be observed that after the transition the light profile at the plasma edge remains approximately constant i.e. the edge density profile does not change, in spite of a substantial increase in the line integrated density.

Fig. 6 shows the Li 2p light profile and the calculated density distribution along the beam close to the chopper time intervals (cf. Fig. 4). As one can see, the light profile and thus the electron density profile in the H-mode becomes extremely flat at the very edge, and very steep around the LCFS. It should be noted that the electron density increases substantially at the LCFS ($\approx$ 60%). This behaviour was found in all analyzed L–H transitions.

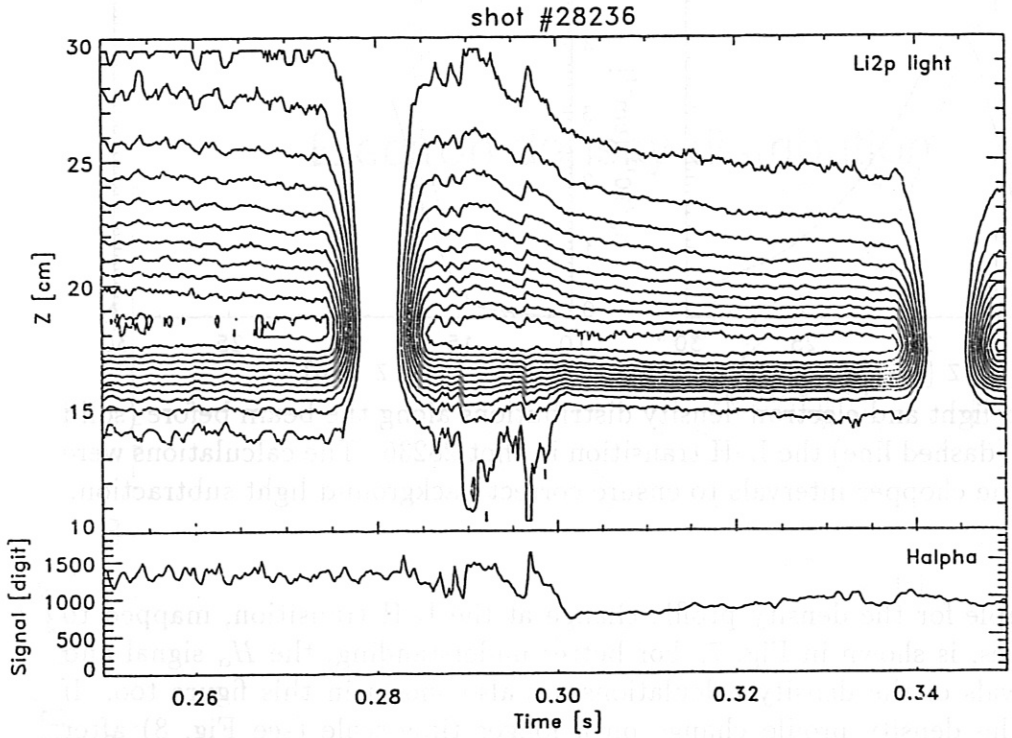

Figure 4: Time evolution of the background subtracted Li 2p light profile (contour plot) and the H_α signal around an L–H transition.

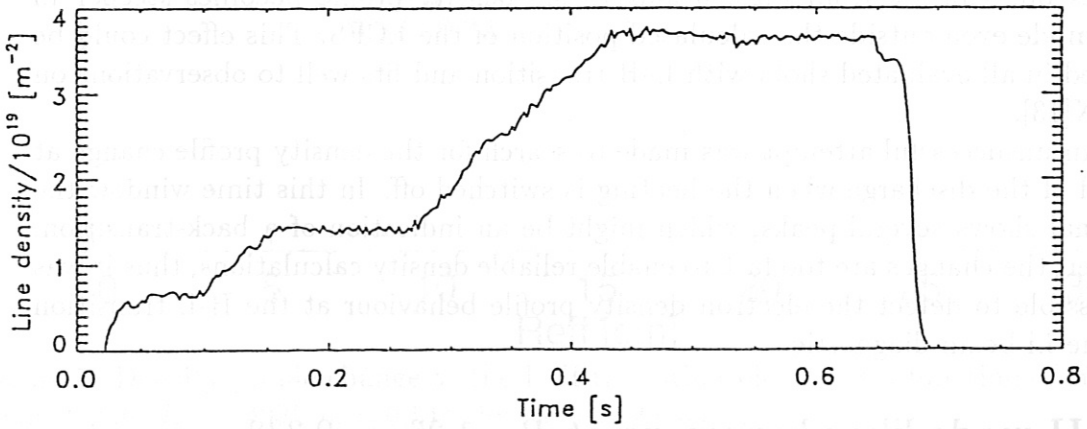

Figure 5: Time evolution of the line integrated electron density in shot 28236. (HCN interferometer diagnostic)

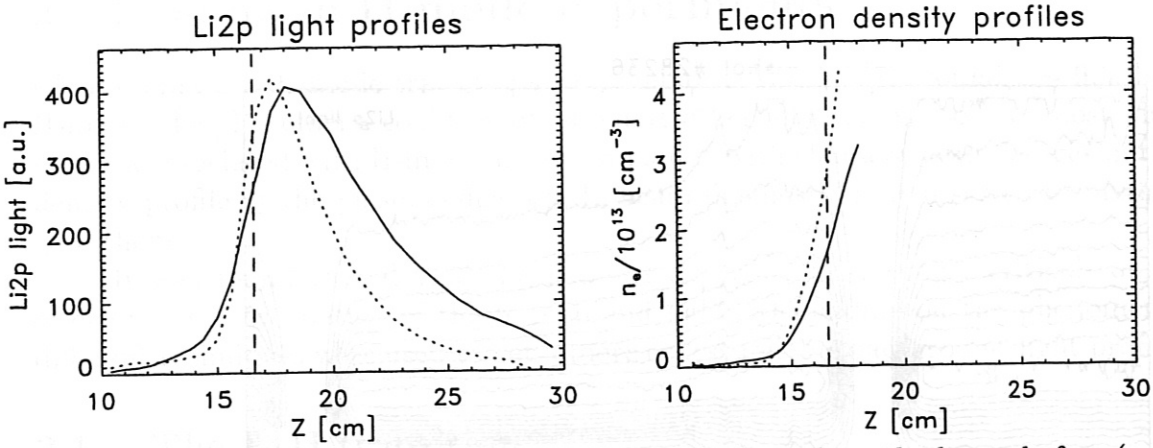

Figure 6: Li 2p light and electron density distributions along the beam before (solid line) and after (dashed line) the L–H transition in shot 28236. The calculations were done close to the chopper intervals to ensure correct background light subtraction.

An example for the density profile change at the L–H transition, mapped to R_{eff} coordinates, is shown in Fig. 7. For better understanding, the H_α signal and the time intervals of the density calculations are also shown in this figure too. If one looks at the density profile change on a longer time scale (see Fig. 8) after the transition, it can be observed that the scrape-off layer profile does not change systematically, while the line averaged electron density increases by a factor of 1.8 in 200 ms, indicating an substantial increase of the core plasma electron density (see Fig 5).

As one can see from Figs. 6 and 7, the density profile becomes steeper in the H-mode even outside the calculated position of the LCFS. This effect could be observed in all evaluated shots with L–H transition and fits well to observations on ASDEX[13].

An unsuccessful attempt was made to search for the density profile change at the end of the discharge when the heating is switched off. In this time window the H_α signal shows several peaks, which might be an indication of a back-transition. However, the changes are too fast to enable reliable density calculations, thus it was not possible to detect the electron density profile behaviour at the H-L transition with the Li-beam diagnostic.

2.2 H-mode like phenomena at B_0=1.26, ι=0.338

In shots 28824–28837 H-mode like signatures ("pseudo H-mode") were observed in the H_α signal. As other diagnostics (e.g. rotation velocity measurement) also reported some H-mode like changes, a detailed analysis was done for these shots.

The first obvious difference between this series and "true" H-mode discharges

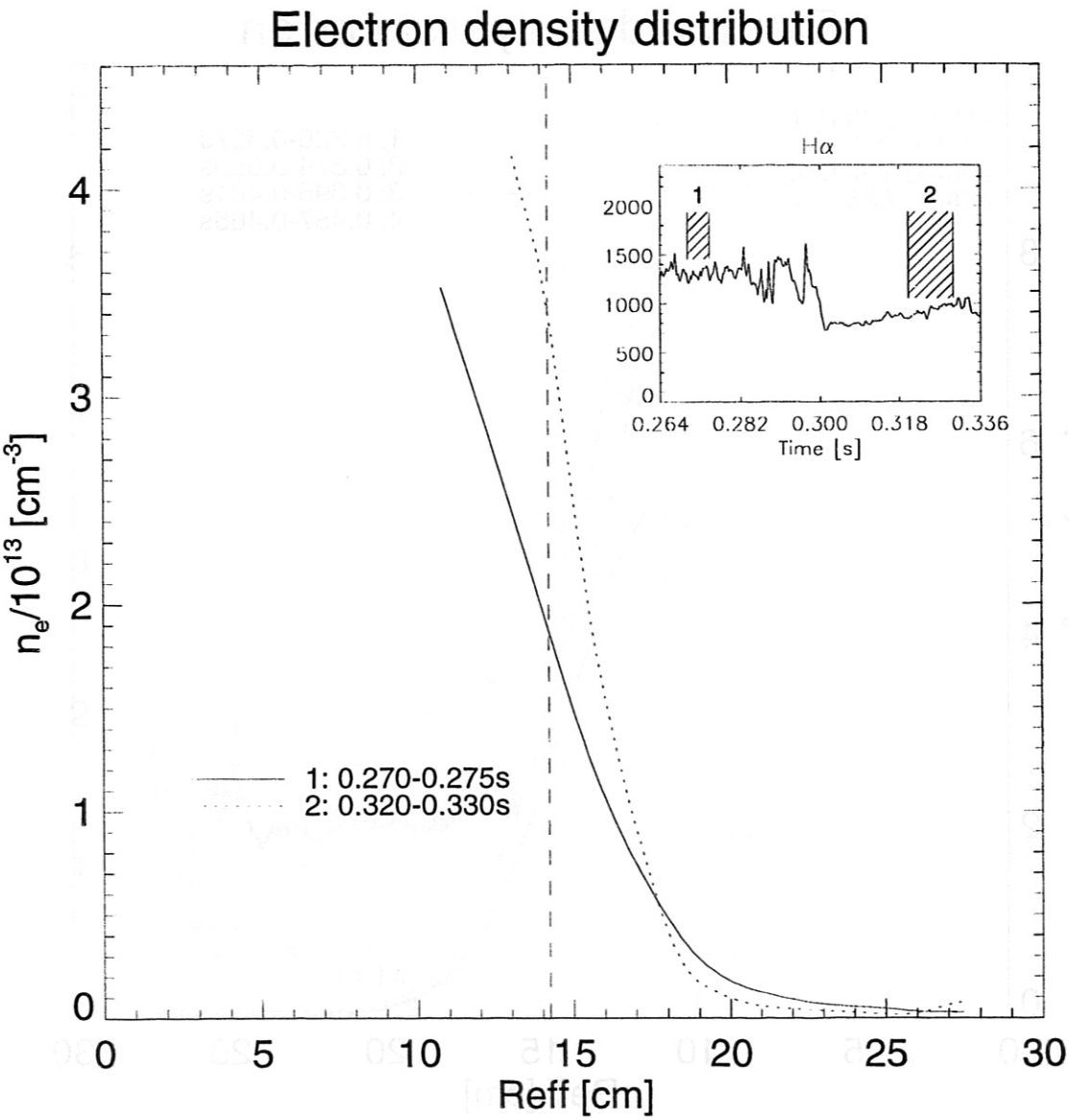

Figure 7: Density profile change at the L–H transition plotted as a function of R_{eff} (shot 28236, B_0=2.49T, $\iota_0 = 0.511$, limiters at 29.4cm).

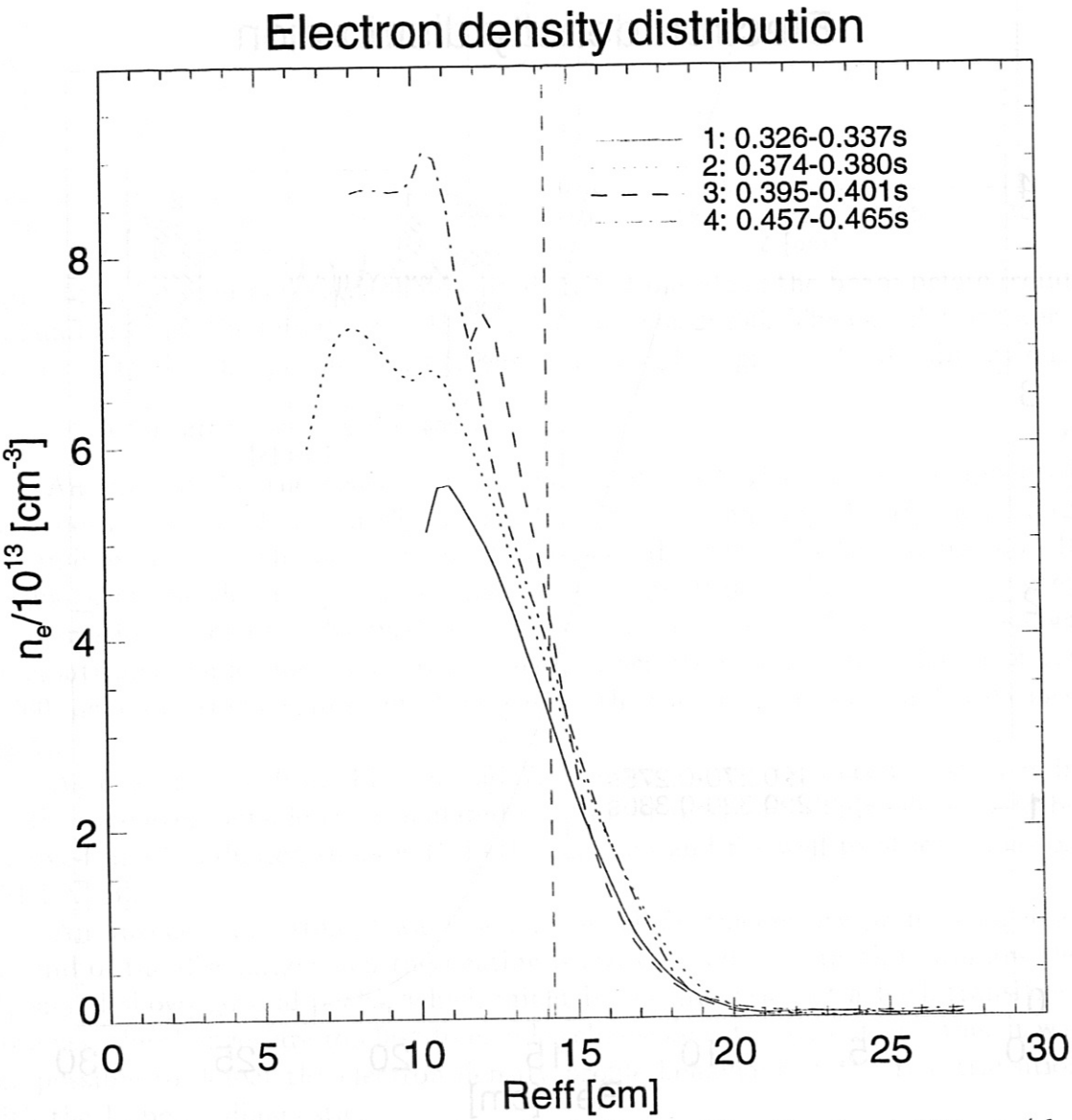

Figure 8: Density profile change after the L–H transition for about 200 ms (shot 28236, B_0=2.49T, $\iota_0 = 0.511$, limiters at 29.4cm).

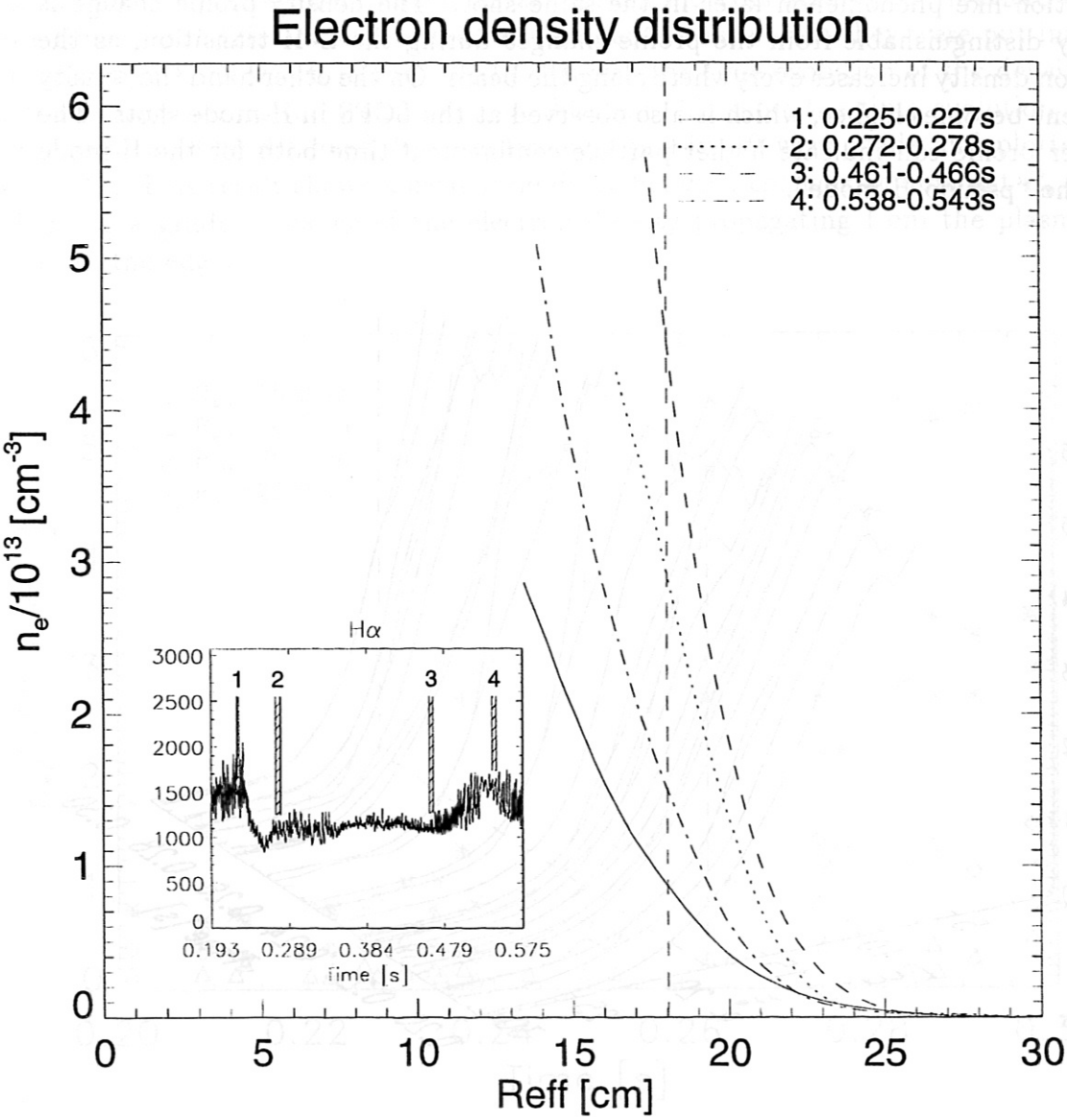

Figure 9: Density profile changes in a "pseudo H-mode" shot (shot 28824, B_0=1.26T, $\iota_0 = 0.338$, limiters at 31.5cm).

is the reproducibility of the phenomenon both in the sense of time evolution and amplitude. The jitter between the time evolutions of H_α or Li-beam signals between "pseudo H-mode" shots was not more than 5ms. Fig. 9 shows the H_α signal and the calculated density profiles before and after the transition and around a back-transition-like phenomenon later in the same shot. The density profile change is clearly distinguishable from the profile changes during the L–H transition, as the electron density increases everywhere along the beam. On the other hand the density gradient becomes higher, which is also observed at the LCFS in H-mode shots. The steeper profile can indicate higher particle confinement time both for the H-mode and the "pseudo H-mode".

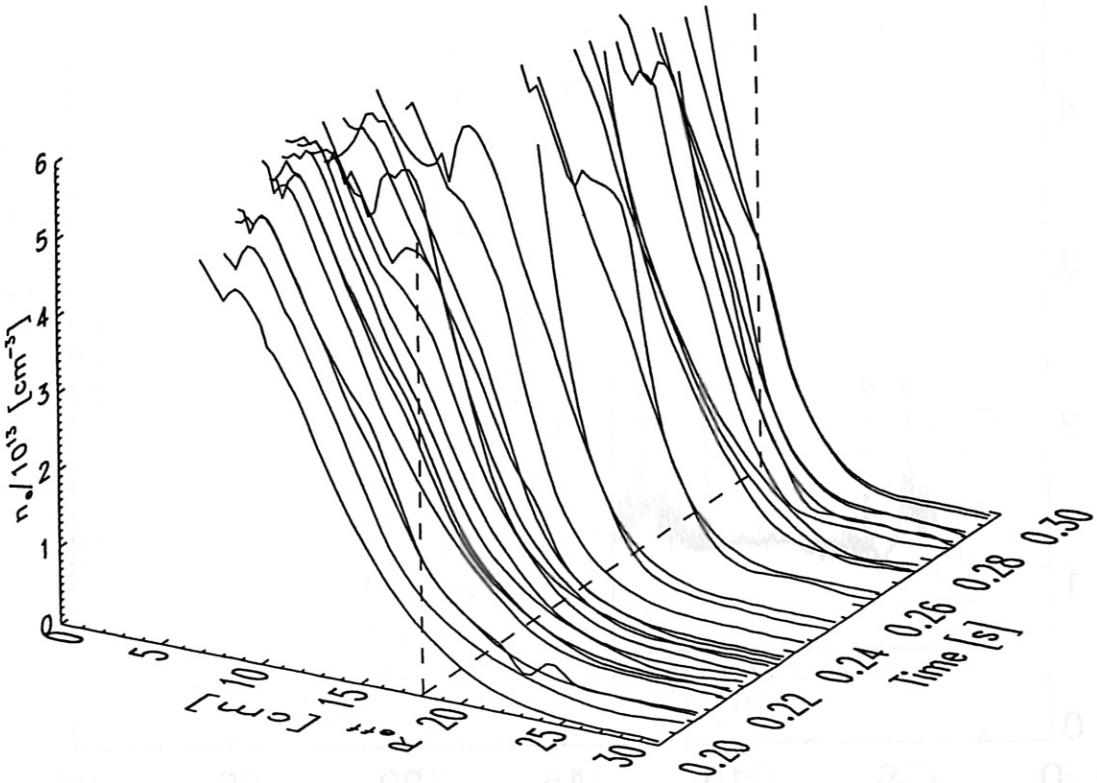

Figure 10: Density profile change during "pseudo H transition". The dashed line represents the position of the LCFS.

Another clear difference from the "true" H-mode is the time scale of the transition. For the H-mode it is about 5ms, while for the present series it is about 30ms. This time is long enough to measure the time evolution of the light profile during the transition, but the background light profile changes dramatically, therefore the

Li 2p light profile can be obtained only close to the chopper intervals. A series of similar shots was available for this phenomenon. Fortunately the chopper times are not synchronized to the beginning of the shot, thus in different shots they occur at different phases of the transition. Electron density distributions were calculated next to the chopper beam-off time intervals in each shot. As density distributions at close times from different shots were very similar to each other, they were put into the same figure, as shown in Fig. 10. In this way the time evolution of the density profile change during the transition was obtained. To show the time evolution of the density at different fixed R_{eff} values, cuts in Fig. 10 were made and plotted in Fig. 11. This result shows a clear time delay between changes at different R_{eff}, indicating a gradual change of the electron density propagating from the plasma center to the edge.

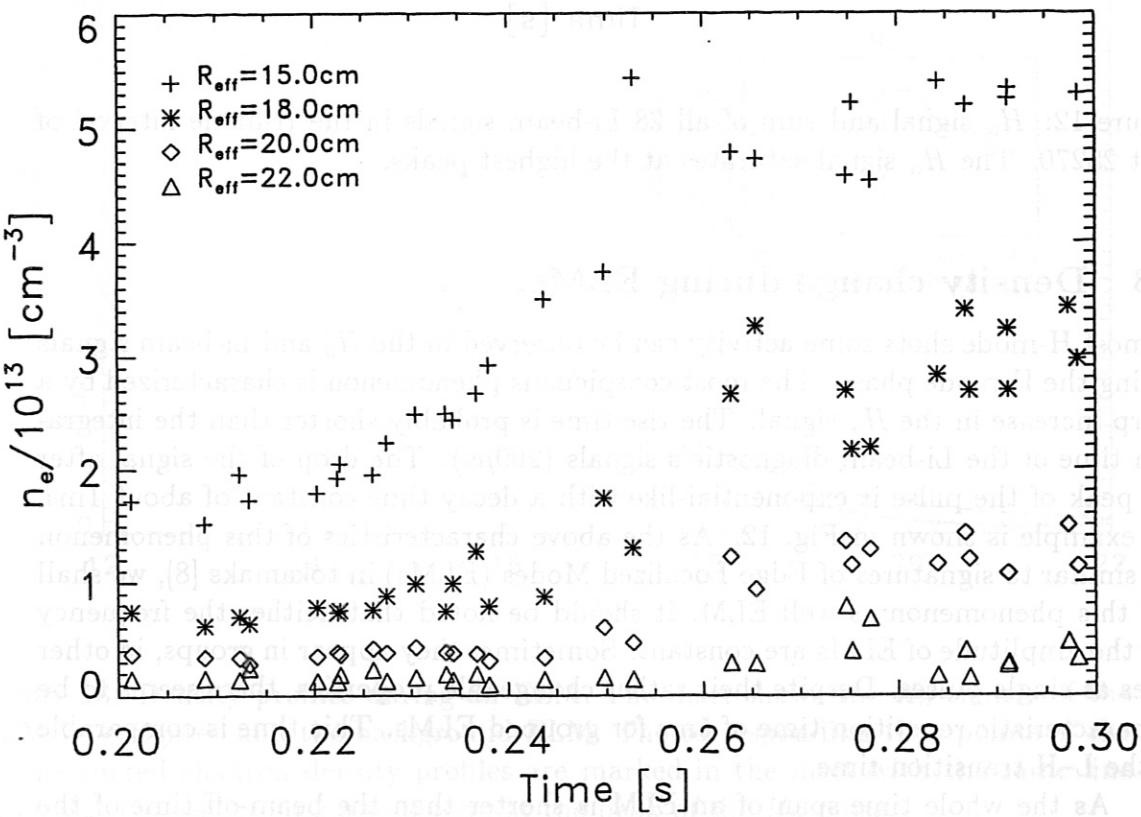

Figure 11: Changes of the electron density at different fixed R_{eff} values during a "pseudo L–H transition".

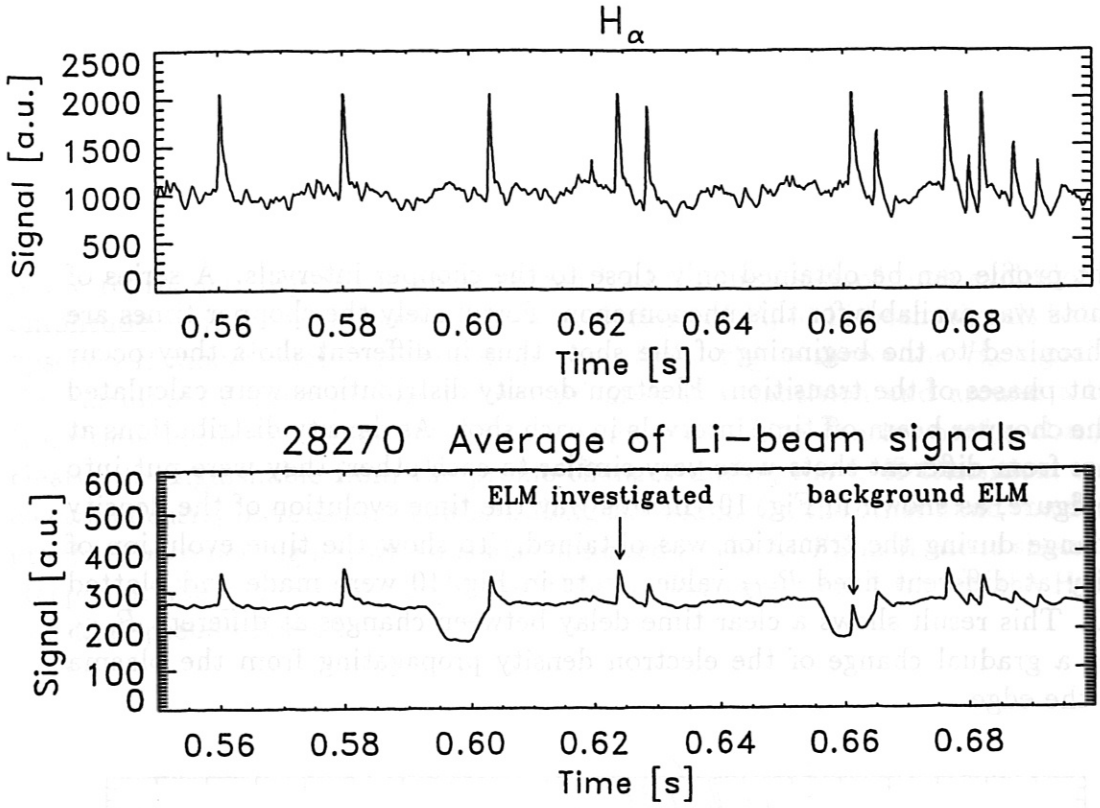

Figure 12: H_α signal and sum of all 28 Li-beam signals in the H-mode interval of shot 28270. The H_α signal saturates at the highest peaks.

2.3 Density change during ELMs.

In most H-mode shots some activity can be observed in the H_α and Li-beam signals during the H-mode phase. The most conspicuous phenomenon is characterized by a sharp increase in the H_α signal. The rise time is probably shorter than the integration time of the Li-beam diagnostic's signals (200μs). The drop of the signal after the peak of the pulse is exponential-like with a decay time constant of about 1ms. An example is shown in Fig. 12. As the above characteristics of this phenomenon are similar to signatures of Edge Localized Modes (ELMs) in tokamaks [8], we shall call this phenomenon as well ELM. It should be noted that neither the frequency nor the amplitude of ELMs are constant. Sometimes they appear in groups, in other cases as single pulses. Despite their rather changeable properties, there seems to be a characteristic repetition time of 5ms for grouped ELMs. This time is comparable to the L–H transition time.

As the whole time span of an ELM is shorter than the beam-off time of the Li-beam chopper, one can try to reconstruct the fast change of the background light, and thus the Li 2p and density profile during an ELM. To do this, two similar ELMs are selected in the same shot, one during beam-on and one during beam-off time, as it is shown in Fig. 12. The light change in the Li-beam channels during the latter pulse is used as background light signal to reconstruct the Li 2p light profile change during the first pulse. The electron density profile change is then calculated from these Li 2p light profile. The time evolution of the two pulses was compared, using the H_α signal as a time reference. Disregarding the saturation of both signals at

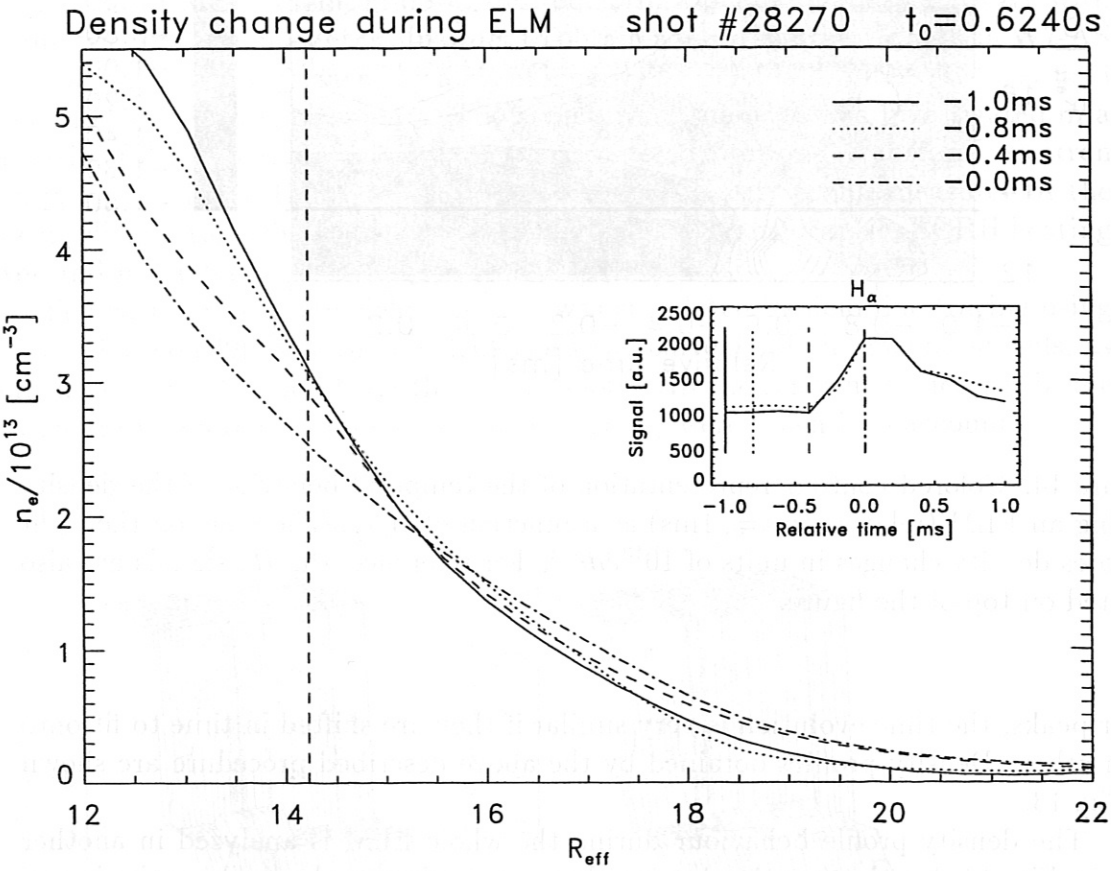

Figure 13: Density profiles during an ELM. The inset shows the H_α signals of the ELM investigated and the background ELM. The corresponding time points of the reconstructed electron density profiles are marked in the inset with the same line type. λ_{n_e} changes from 2.0 to 3.4 cm at the peak of the H_α pulse.

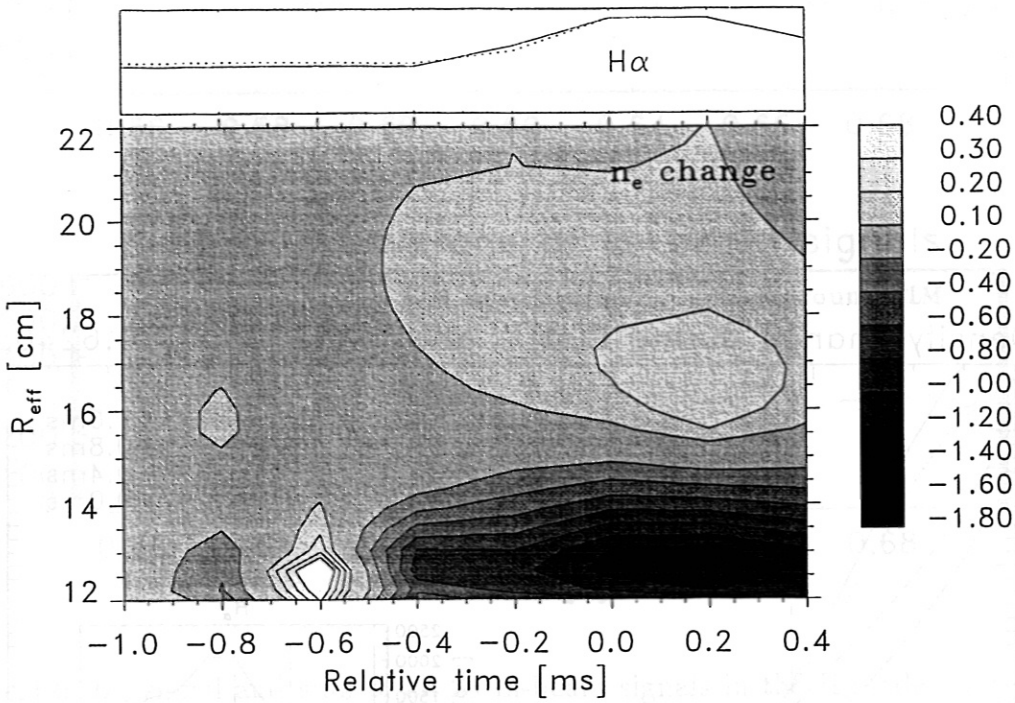

Figure 14: Colored contour representation of the temporal behavior of the density during an ELM (relative to t= -1ms) as a function of R_{eff}. The scale on the right denotes density changes in units of $10^{13} cm^{-3}$. For reference, the H_α signals are also plotted on top of the figure.

their peaks, the time evolution is very similar if they are shifted in time to fit onto each other. Density profiles obtained by the above described procedure are shown in Fig. 13.

The density profile behaviour during the whole ELM is analyzed in another way in Fig. 14, by plotting the density change at different places along the beam. As one could see from the previous figures, there is a density decrease at the inner channels, while there is an increase on the outer ones. The change between the first and the last profile in Fig. 13 resembles very much that of a reversed L–H transition. After the peak of the H_α pulse, the density profile returns to the pre-ELM one.

3 Density profiles in W7–AS with poloidal limiters

3.1 General

The plasma in W7–AS can be both separatrix or limiter bounded. In the limiter bounded case the two main up-down limiters form a Scrape Off Layer (SOL) with asymmetric connection lengths. In order to obtain a more symmetric SOL in W7-AS the main limiters were replaced by a set of inner-lying poloidal limiters (two per field period) for a serie of experiments. The structure of the edge was investigated in a long serie of discharges varying different parameters (rotational transform, electron density, ...). In this section the behaviour of the edge density profile measured by the Li-beam diagnostic is discussed for different rotational transform (ι), ECRH heating power and line integrated density.

The vacuum magnetic field topology was calculated by field line tracing using the Gourdon code[9]. For these calculations the currents of the magnetic coils, as input data, were obtained from the actual shots. All the relevant structures inside the vacuum vessel (e.g. limiters, antennas, ... etc.) were taken into account.

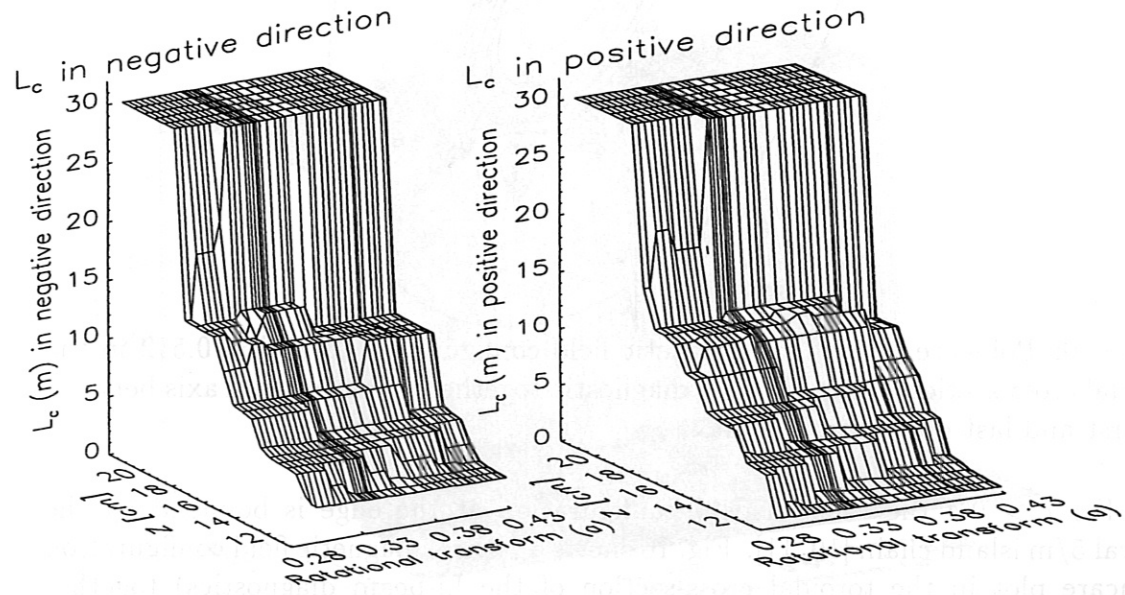

Figure 15: Connection length along the Li-beam vs edge rotational transform. The $L_c \geq 30$m values denote the infinite connection length of the core plasma.

For $\iota \leq 0.4$ the edge topology is determined by the inner limiters (in this case typically a vertical field was applied to push the plasma against the inner limiters and protect the outer part of the vessel wall from contact with the plasma), leading

to a smooth variation of the connection length in the SOL as a function of rotational transform. Fig. 15 shows Gourdon code calculated vacuum field connection lengths at the Li-beam diagnostic's observation points as a function of iota. One can realize from Fig. 15 that the radial position of the LCFS does not change considerably as a function of iota. Outside of the LCFS one can find a approximately 2 cm wide range in the Z coordinate with a nearly constant connection length of 12 m in both directions.

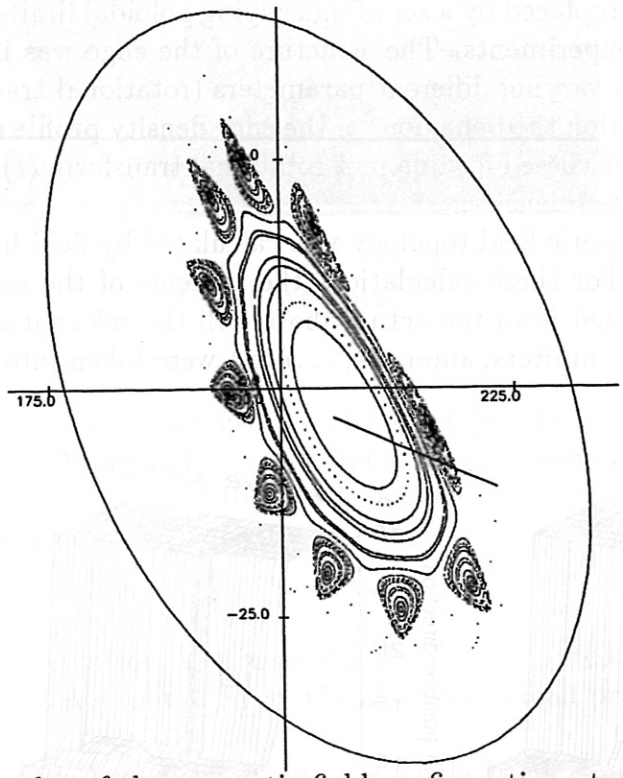

Figure 16: Poincare plot of the magnetic field configuration at $\iota(a) = 0.512$ in the poloidal cross-section of the Li-beam diagnostic together with the beam axis between the first and last observation point.

For $\iota > 0.4$ the vacuum field configuration at the edge is bounded by the natural 5/m island chain [10, 11]. Fig. 16 shows a typical magnetic field configuration (Poincare plot in the toroidal cross-section of the Li-beam diagnostics) together with the beam axis for $\iota(a) = 0.512$ (coil currents from shot #29296). The 5/10 islands are partially intersected by the limiters, introducing finite connection lengths between the islands and the main plasma. The Li-beam crosses one of these islands between the O and X points. Fig. 17 shows the calculated connection length for this rotational transform range ($0.4 < \iota(a) < 0.65$) in both directions. The vacuum edge topology (the radial position and width of the islands, the radial variation of the connection length and the position of the LCFS) highly depends on the rotational

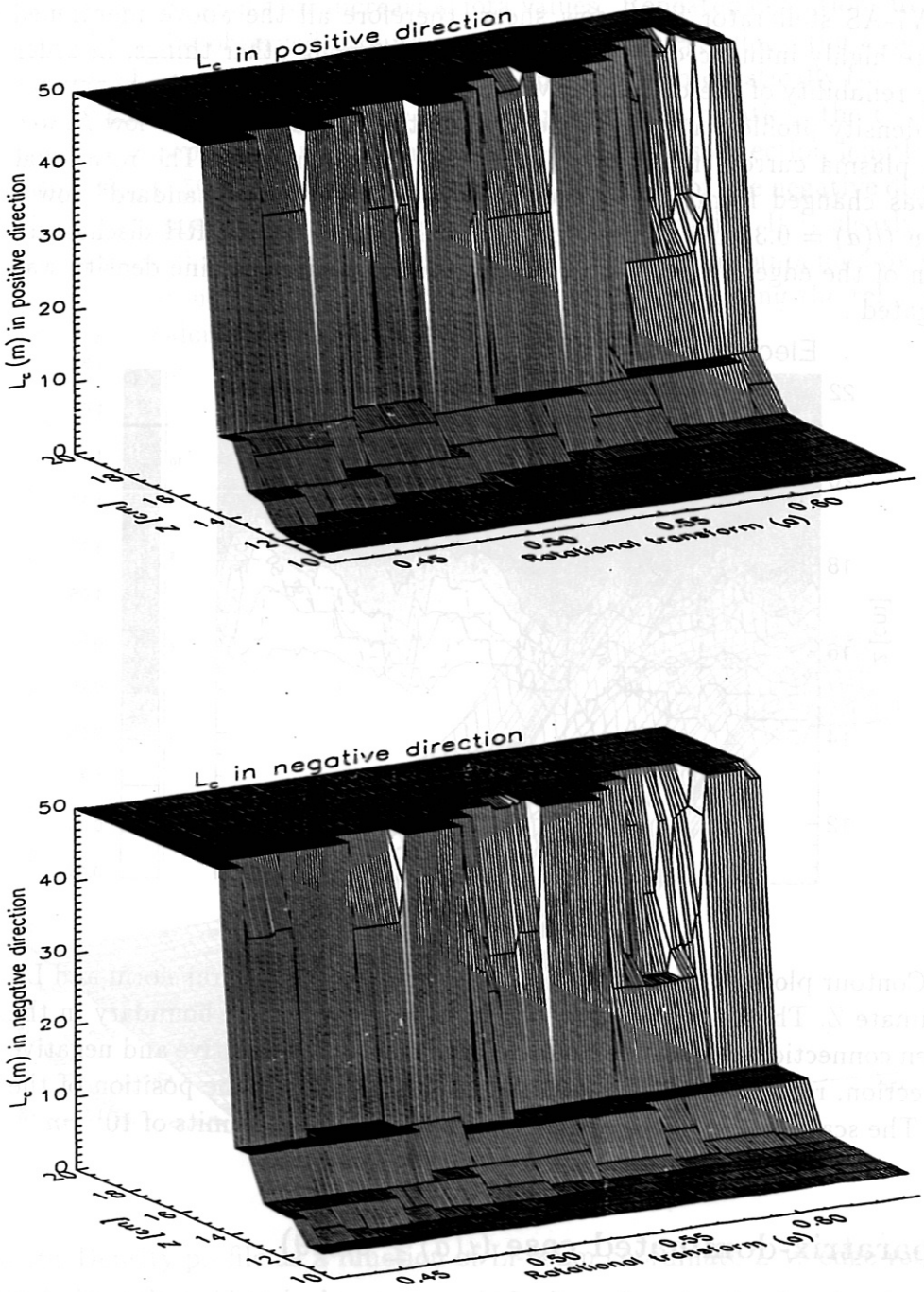

Figure 17: The Gourdon code calculated connection length along the Li-beam coordinate Z *vs* edge rotational transform ($\iota(a)$).

transform, as it is shown in this figure.

The W7-AS stellarator has a low shear, therefore all the above mentioned quantities are highly influenced by plasma currents. Among other things, in order to verify the reliability of the calculated vacuum field edge topology, the behaviour of the edge density profile was investigated in a detailed iota scan with low β, low density, net plasma current free, $B_0 = 1.25T$, ECRH discharges. The rotational transform was changed from 0.29 to 0.64. In addition for the "standard" low ι configuration ($\iota(a) = 0.34$ net current free, $B_0 = 2.5T$, flat top ECRH discharges) the variation of the edge density profile versus heating power and line density was also investigated .

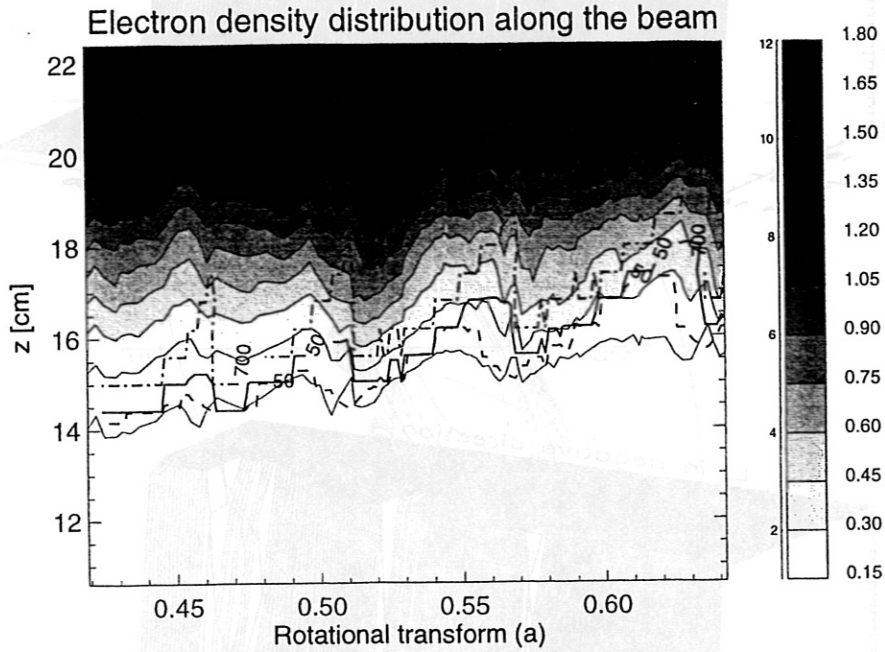

Figure 18: Contour plot of the electron density *vs* edge rotational transform and Li-beam coordinate Z. The thick solid and dashed lines represent the boundary in the SOL between connection lengths of less/more than 50 m in the positive and negative toroidal direction, respectively. The dash-dotted line represents the position of the separatrix. The scale on the right denotes the electron density in units of $10^{13} cm^{-3}$.

3.2 Separatrix-dominated case ($\iota(a) \geq 0.419$)

The electron density distribution along the Li-beam was calculated in a time window of 0.3-0.35 sec for all shots from 29293 to 29407. The electron temperature profile for the density reconstruction was obtained from Thomson scattering (shot 29377). All of these electron density profiles are plotted as a contour plot in Fig. 18. Choosing other time windows in the plateau phase of the discharge for the same series of shots, reveal identical behaviour of the electron density profile. One can see in Fig. 18, that

the plasma globally shrinks for increasing iota values. Repeated deviations from this general trend can be observed around resonant $\iota(a)$ values, where the appearance of 5/m islands change the edge magnetic field configuration drastically ($\iota(a)$=0.463, 0.512, 0.57, 0.635). Derived from the connection length calculation, the thick solid line in this figure represents the radial position where the connection length in the positive direction is 50 m. The dashed line shows the same for the negative direction. The dash-dotted line represents the position of the separatrix. It is clearly shown that characteristic changes in the position of these lines are accompanied by similar changes in the contour lines of the density in the SOL, supporting the reliability of the vacuum field calculation.

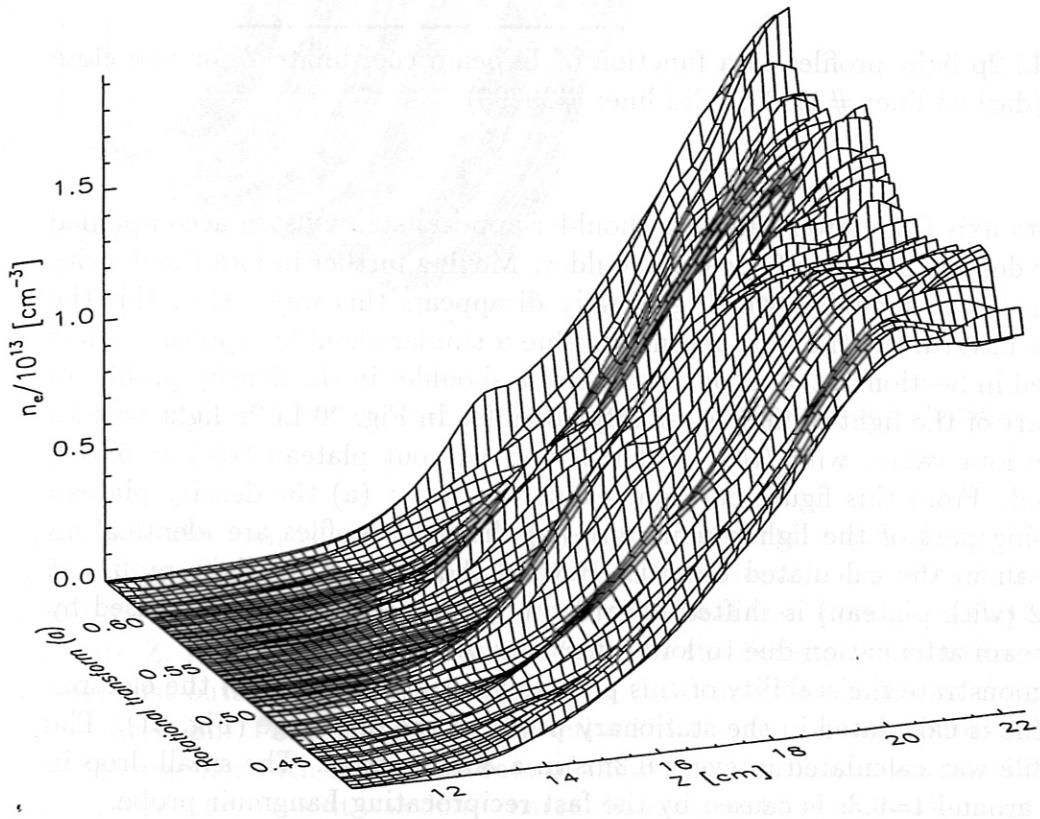

Figure 19: Density profile as a function of Li-beam coordinate Z *vs* edge rotational transform.

The density variation in the gradient region as a function of rotational transform is plotted in Fig. 19 as a three dimensional plot. The same data set was used as in Fig. 18. One can again see the dramatic changes of the density profile around the resonant iota values. In order to demonstrate these changes the variation of the profile around $\iota(a) = 0.5$ is investigated in detail as the best example. Moving

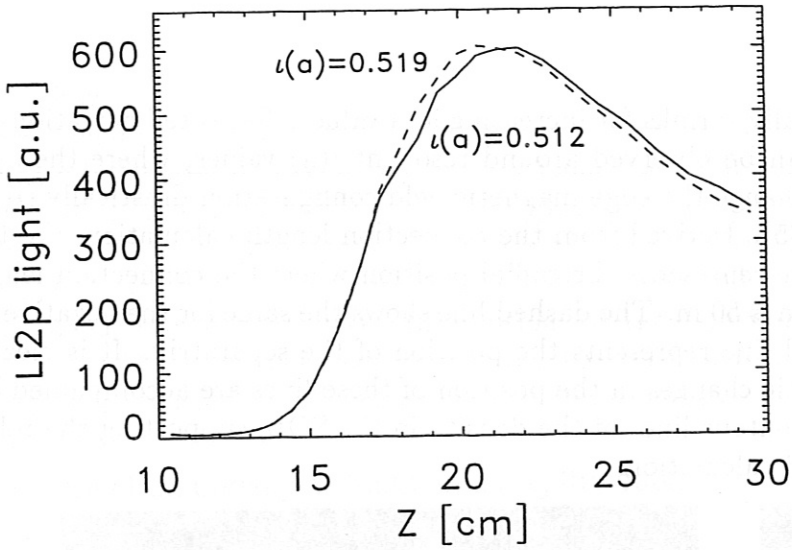

Figure 20: Li 2p light profiles as a function of Li-beam coordinate Z for two close iota values (dashed line: #29300, solid line: #29296).

along the iota axis from lower values, a shoulder appears step by step accompanied by a steeper density profile outside the shoulder. Moving further in iota the density increases inside the shoulder, which gradually disappears this way. After this the profile shifts inward. At the next resonant value a similar shoulder appears. As it was discussed in Section 1, the reconstruction of a shoulder in the density profile, in the rising part of the light profile, is reliably possible. In Fig. 20 Li 2p light profiles at two close iota values with ($\iota(a) = 0.512$) and without plateau ($\iota(a) = 0.519$) are compared. From this figure one can realize two facts: (a) the density plateau is in the rising part of the light profile and (b) the light profiles are identical up to the plateau in the calculated density. Beyond the plateau the light profile at $\iota(a) = 0.512$ (with plateau) is shifted toward the plasma center. This is caused by a lower Li-beam attenuation due to lower densities in the plateau region.

To demonstrate the stability of this plateau the time evolution of the electron density profile is calculated in the stationary phase of the discharge (Fig. 21). The density profile was calculated in every 0.2ms in a 300ms range. The small drop in the density around t=0.3s is caused by the fast reciprocating Langmuir probe.

One might explain the appearance of the plateau with the presence of the 5/m islands[15] partly intersected by the limiters, as they introduce a radial short cut in the particle and energy transport by a strong parallel component. The radial position of the plateau agree well with the position of the vacuum field calculated islands. Closed islands (inside the separatrix of the main plasma) appear at $\iota(a)$ values slightly higher than the values listed above. However, their radial size is smaller and they are located deeper in the plasma, therefore the plateau, if it exists in this case at all, can not be reconstructed, as discussed in Section 1.

The KW equilibrium code, which calculates the flux coordinates, does not take

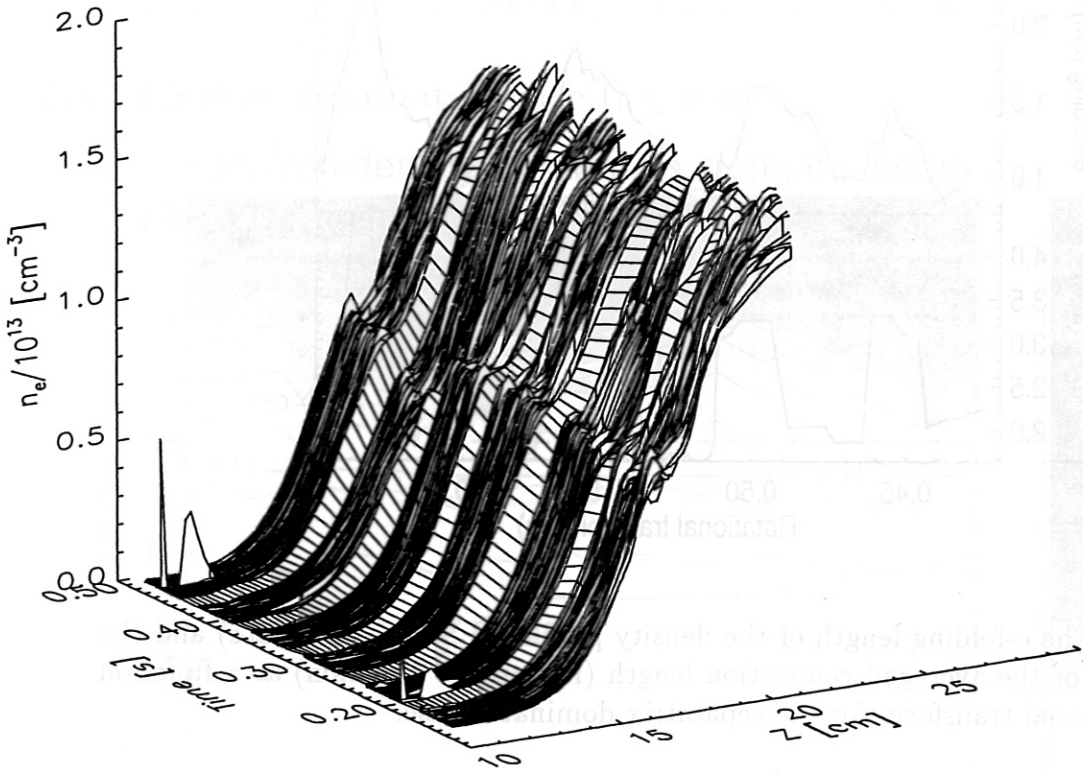

Figure 21: Time evolution of the density profile in shot #29296.

into account the 5/m island chain, therefore the parametrisation of the density in flux coordinates is not possible in the SOL for all rotational transforms in the range in question. Therefore we can investigate only the local transport using the Li-beam coordinate Z. An exponential curve was fitted to the density distribution in a 3.5 cm range just outside the 50m contour line of the connection length in the positive toroidal direction. The e-folding lengths derived by this fitting procedure are plotted in Fig. 22 together with the square root of the connection length averaged over the same Z range where the fit was done. Large changes can be observed in the e-folding length correlated with the structure of the density distribution and the variation of the average connection length. Four maxima appear in both curves close to the resonant $\iota(a)$ values mentioned above.

One can plot the fitted e-folding length as a function of the square root of the averaged connection length for all iota values in this range as it is shown in Fig. 23 . Using a simple axisymmetric SOL model (see e.g. [12]), and supposing that the perpendicular particle diffusion coefficient and the electron temperature do not depend on the rotational transform in the considered range, one finds a linear relation between the square root of the connection length and the e-folding length

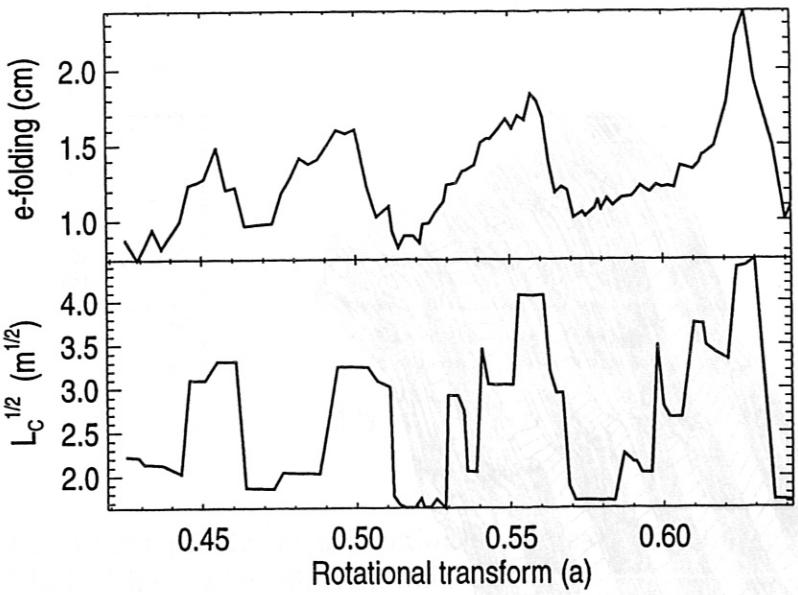

Figure 22: The e-folding length of the density profile (in beam coordinate) and the square root of the averaged connection length (in positive direction) as a function of the rotational transform for the separatrix dominated case.

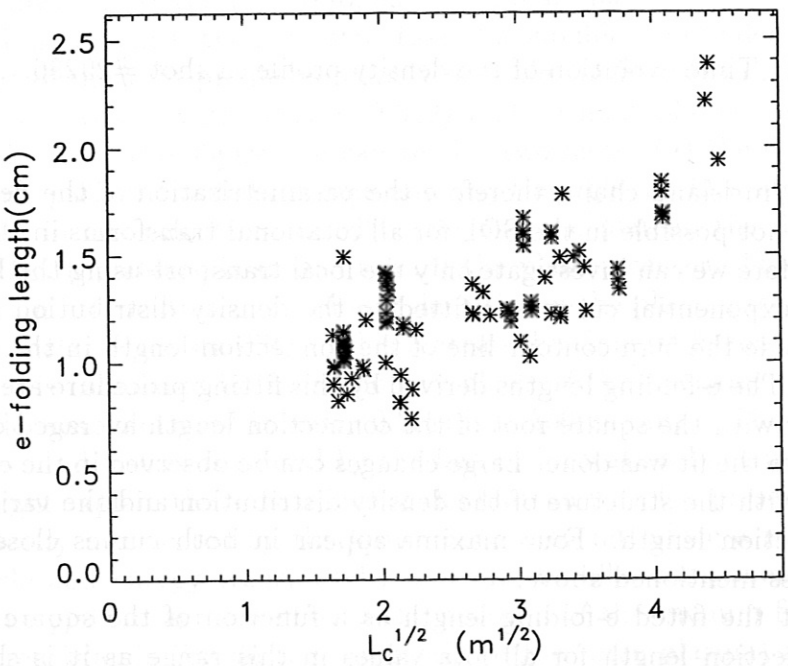

Figure 23: The e-folding length of the density profile (in beam coordinates) as a function of the square root of the averaged connection length (in positive toroidal direction) .

of the electron density. The results in Fig. 23 do not contradict this consideration.

3.3 Limiter-dominated case ($\iota \leq 0.4$)

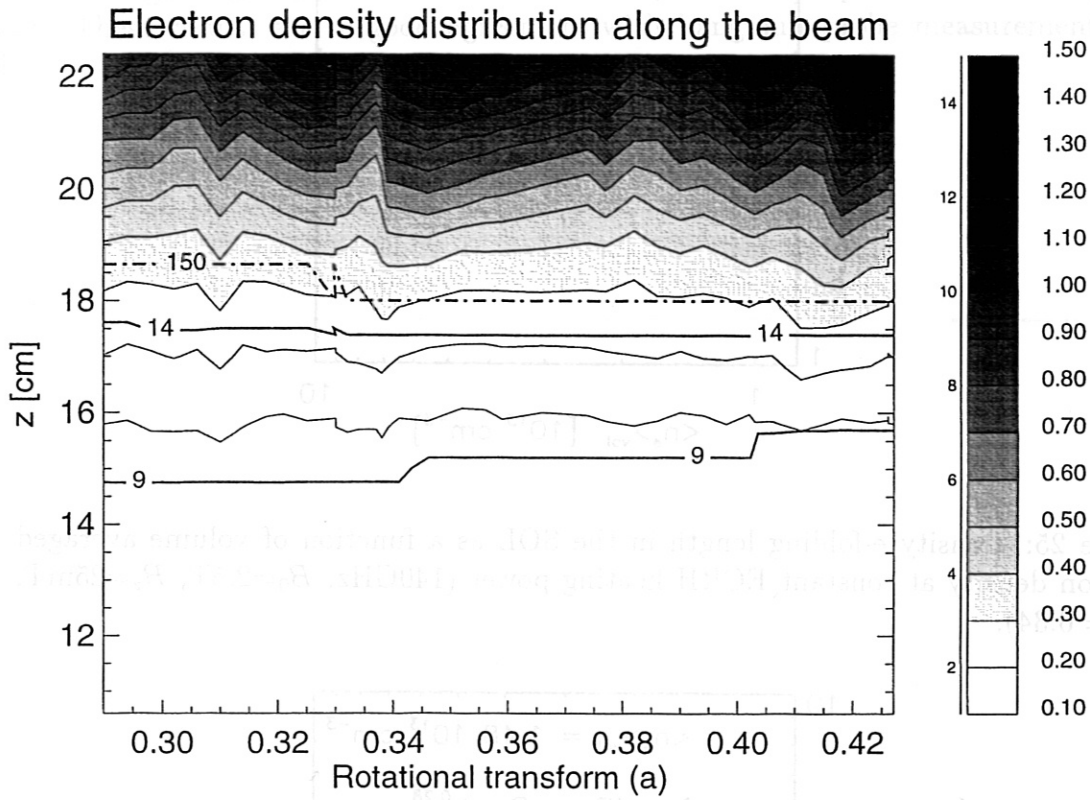

Figure 24: Contour plot of the electron density *vs* edge rotational transform and Li-beam coordinate Z. The solid lines represent contour lines of the connection length (the connection length is indicated). The numbers on the right side of the grey scale represents the electron density in $10^{13} cm^{-3}$. The dash dot line shows the position of the LCFS.

For the limiter dominated case ($\iota \leq 0.4$) the plasma was shifted inside by applying a vertical magnetic field. Therefore a significantly lower electron density is measured at the same Z values compared to the values in Fig. 18, as it can be seen in Fig. 24. This figure shows density profiles as a function of Li-beam coordinate Z *vs* the rotational transform. In this rotational transform range neither the density profile nor the vacuum field calculated connection length changes drastically in the SOL. Investigating the density e-folding length in the SOL of these profiles (both in Li-beam coordinates and in flux coordinates) one finds a slight decrease with increasing rotational transform.

Density e-folding lengths in the SOL (in flux coordinates) for a density scan with constant ECRH heating power (140GHz, P=460kW, B_0=2.5T, B_z=25mT,

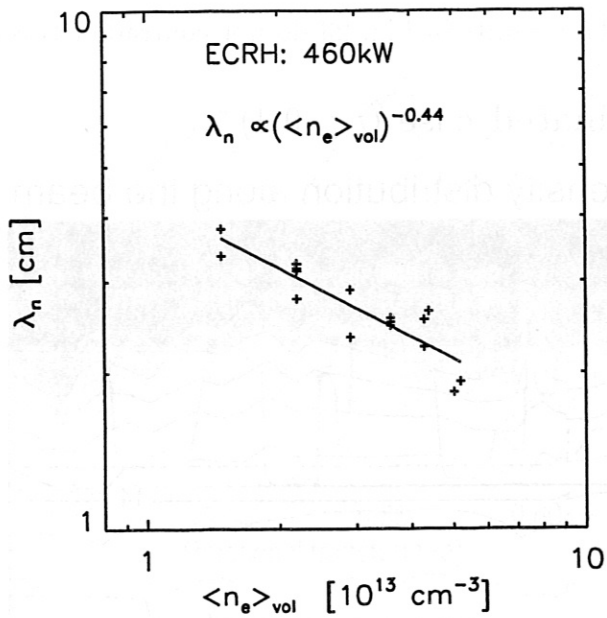

Figure 25: Density e-folding length in the SOL as a function of volume averaged electron density at constant ECRH heating power (140GHz, B_0=2.5T, B_z=25mT, $\iota(a) = 0.34$).

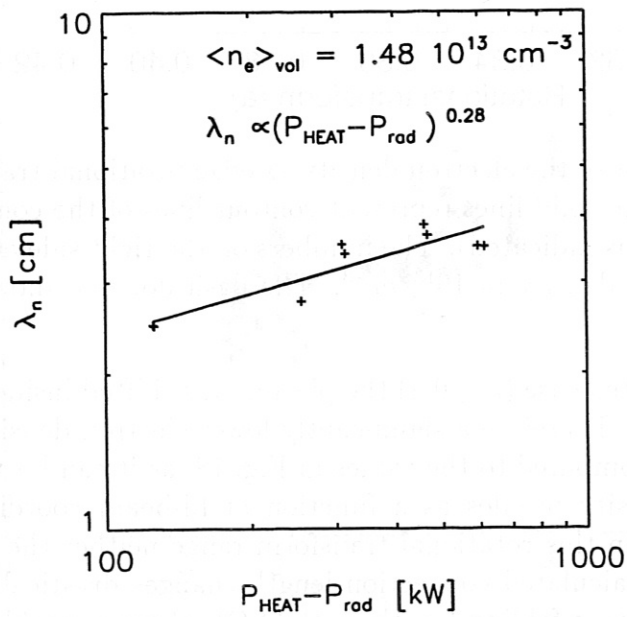

Figure 26: Density e-folding length in the SOL as a function of the non-radiated part of the heating power at constant volume averaged density (70/140GHz, B_0=2.5T, B_z=17 mT, $\iota(a) = 0.34$).

$\iota(a) = 0.34$) and for a power scan with constant volume averaged density (70/140GHz, B_0=2.5T, B_z=17 mT, $\iota(a) = 0.34$, $\langle n_e \rangle_{vol} = 1.48 \times 10^{13} cm^{-3}$) are shown in Fig. 25 and in Fig. 26. The e-folding length decreases with increasing volume averaged density and increases with the non-radiated part of the heating power. These results are in good agreement with Langmuir probe measurements [14].

4 Observation of density fluctuations

4.1 Measurements

The Li-beam diagnostic measures the time evolution of local electron density at multiple points along the Li-beam, therefore it can also detect electron density fluctuations. As the Li-beam (Li-IXS) measurement channels are smoothed with a 0.2 ms RC time constant, only fluctuations having a longer characteristic time than this value can be detected. In other words, the frequency range of the fluctuation measurement by the Li-beam diagnostic is limited to approximately 5 kHz. In the same way, the spatial integration and separation of the channels gives a lower limit on the detectable structure size, which is about 0.6 cm in the SOL and 1 cm in the core plasma. In addition to these two limitations, a third one is present due to the lifetime of the Li 2p atomic level as it has been discussed in Section 1.

The first step to investigate fluctuations is to look at the time evolution of the Li 2p light profile. An example is shown in Fig. 27 for a shot with closed limiters (large scrape-off layer).

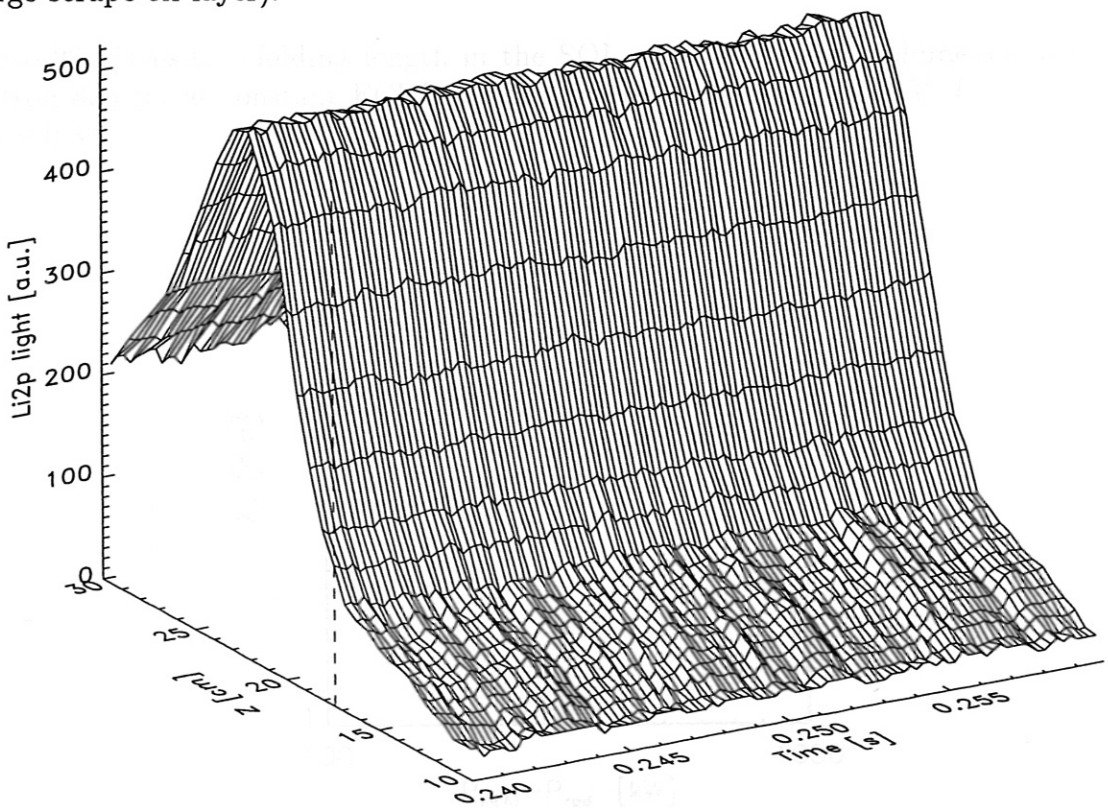

Figure 27: Li 2p light intensity *vs* beam coordinate Z and time for shot #27165 (B_0=1.27T, ECRH, $\iota_a = 0.344$, $\int n_e dl = 5 \times 10^{18} m^{-2}$), showing correlated fluctuations at the edge. The dashed vertical line represents the position of the LCFS.

As one can immediately see from this figure, there are temporal structures in

the Li 2p light signals correlated across the whole SOL ($\Delta Z \sim 5cm$). As the fluctuation amplitude is less by a factor of about 5 in the background light of the plasma and their fluctuations show no cross-correlation between channels, the structures in Fig. 27 should be fluctuations in the Li 2p light emitted from the Li-beam. As the fluctuations are correlated across several channels, their origin cannot be photon statistical noise. This is also supported by the fluctuation amplitude distributions (see Fig. 28) as the photon statistical noise amplitude ought to be proportional to the square root of the signal amplitude. In contrast to this, the fluctuation amplitude is constant or even higher in the SOL.

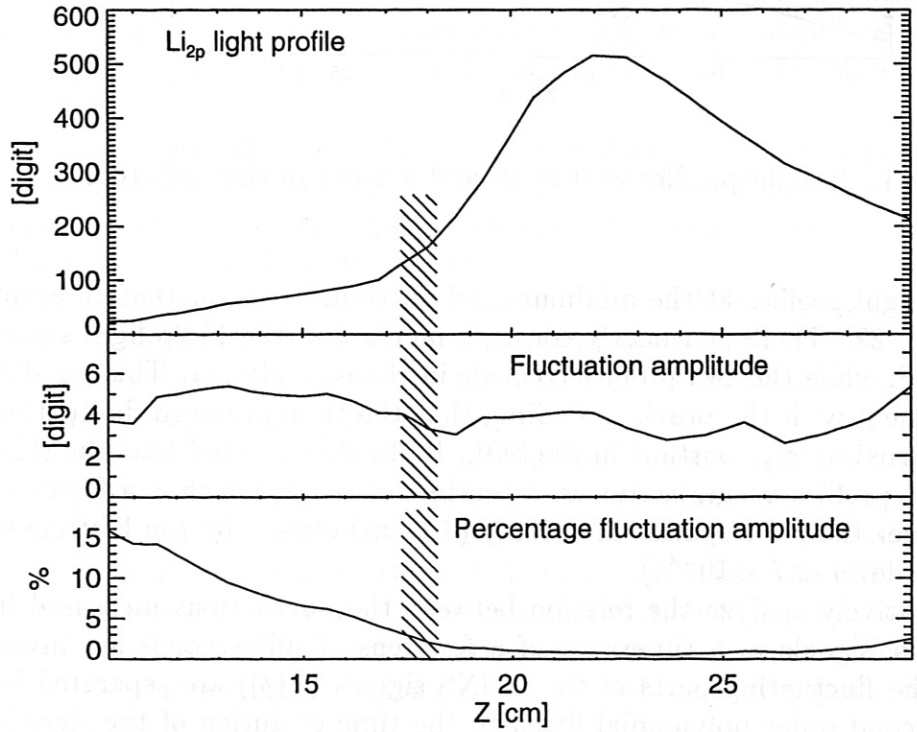

Figure 28: Li 2p light profile, its absolute and percentage fluctuation amplitude as a function of the Li-beam coordinate Z. The hatched area marks the calculated position of the LCFS taking into account inaccuracies in plasma beta.

One might argue that correlated changes in the light signals could be caused by changes in the Li-beam intensity. However, such a change should cause the same percentage modulation of the signals everywhere along the Li-beam, in contrast to the measured percentage fluctuation levels which change by a factor of 10 along the Li-beam. Li-beam intensity fluctuations should also cause changes correlated between the Li-IXS signals and the "neutral density signal", which is clearly not the case as it is shown in Fig. 30.

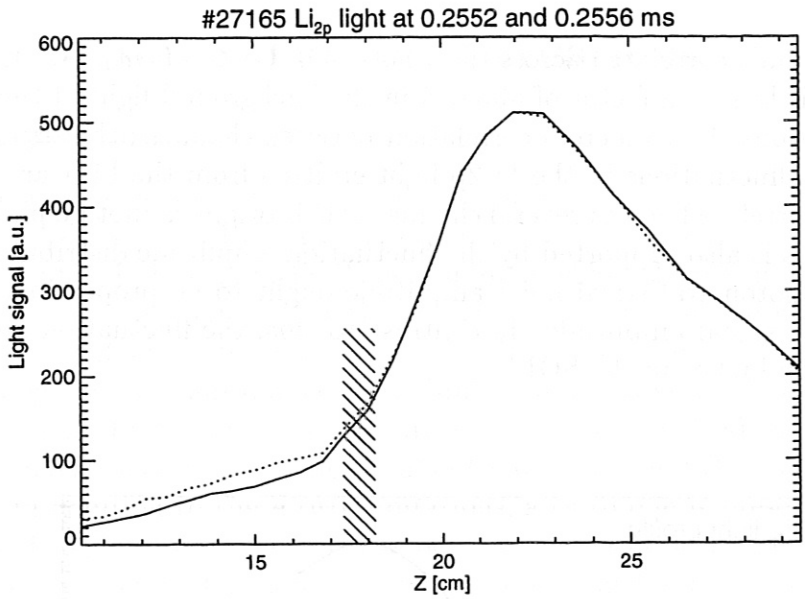

Figure 29: Li 2p light profiles at 0.2552s and 0.2556s in shot #27165.

The Li 2p light profiles at the minimum and maximum of a fluctuation event are shown in Fig. 29. There is a nearly constant increase in the Li 2p light signal outside the LCFS, while the two profiles coincide in the core plasma. This parallel shift is in agreement with the previous finding, that the time averaged fluctuation amplitude is approximately constant in the SOL. It should be noted that the shift in the Li 2p light profiles occurs across an 8 centimeter range, which is a factor of nearly three longer than the spatial smoothing (3.1 cm) caused by the lifetime of the excited Li 2p level ($2.7 \times 10^{-8} s$).

To quantitatively analyze the relation between the fluctuations measured in different channels, signals in a timerange of a few tens of milliseconds are investigated. First the fluctuating parts of the Li-IXS signals ($S(t)$) are separated by subtracting a second order polynomial fitted to the time evolution of the signals. This procedure removes average values and slow drifts from the signals. Zero time delay cross-correlation functions of the form

$$C_i(j) = \frac{\int_{t_1}^{t_2} S_i(t) S_j(t) dt}{\sqrt{\int_{t_1}^{t_2} S_i^2(t) dt \int_{t_1}^{t_2} S_j^2(t) dt}}$$

are calculated, where $S_i(t)$ and $S_j(t)$ are the fluctuating parts of the signals in channels i and j, respectively. (t_1, t_2) is the time interval investigated. From the above definition one can see, that $C_i(i) = 1$ for all i. By substituting variable j and i with the Z coordinate of the channels one gets two-dimensional cross-correlation functions $C(Z_1, Z_2)$ describing the cross-correlation between the fluctuations at Z_1 and Z_2 positions along the Li-beam coordinate. Fig. 30 shows some of these cross-

correlation functions for different fixed Z_1 for two shots, one with open and one with closed limiters. One can clearly see that the correlation length along Z changes as the limiter position is changed. The correlated fluctuations are confined to the SOL. For several cross correlation functions, a negative correlation can be observed between the SOL channels and the channels deeper in the plasma. This behavior will be discussed below.

The cross-correlation functions of the H_α signal (Li-diagnostic) and the neutral density signal with all Li-IXS signals are also plotted in Fig. 30. Neither the H_α nor the neutral density signal show correlation with the fluctuations of the Li-IXS signals.

One can calculate the cross-correlation functions for different time delays and search for the propagation of the observed fluctuations. This was attempted, but no clear time delay was observed between fluctuations at different Z values. This means, that the channel to channel propagation time of the fluctuations is shorter than the signal sampling period time.

Photon statistical noise and beam current fluctuations were already ruled out above as possible sources of the observed fluctuations. It is clear that electrical amplifier noises can also be ruled out, as there is no correlation of the Li-IXS signals with the H_α and neutral density signals.

The above considerations show that the observed fluctuations of the Li-IXS signals are caused by fluctuations of plasma parameters. As the electron temperature and Z_{eff} have very small effect on the Li 2p light intensity, the observed fluctuations are most likely caused by electron density fluctuations.

In order to determine if the fluctuations are caused by electron-cyclotron heating of the plasma, the fluctuation level and correlation functions were compared just before and after the heating was switched off at the end of the discharge. Although the density profile responds to the switch-off within 5 ms, there is no change in the relative fluctuation level or in the cross-correlation functions. This fact indicates that the observed density fluctuations are not connected to effects caused by electron cyclotron heating, meaning they are probably not transport relevant.

4.2 Simulation of density fluctuations and discussion

As was mentioned in Section 1, the connection between the electron density and the Li 2p light profile is not local, i.e. the light intensity at a given point is a function of the whole electron density distribution from the plasma edge up to the point in question. As a consequence, if there are fluctuations in the electron density distribution localized at one point, the Li 2p light profile shows fluctuations at other places too. In other words, cross-correlation between fluctuations in the Li 2p light signals at different places do not automatically correspond to correlations in the density fluctuations at the same places.

To overcome this problem, one might wish to unfold the electron density distri-

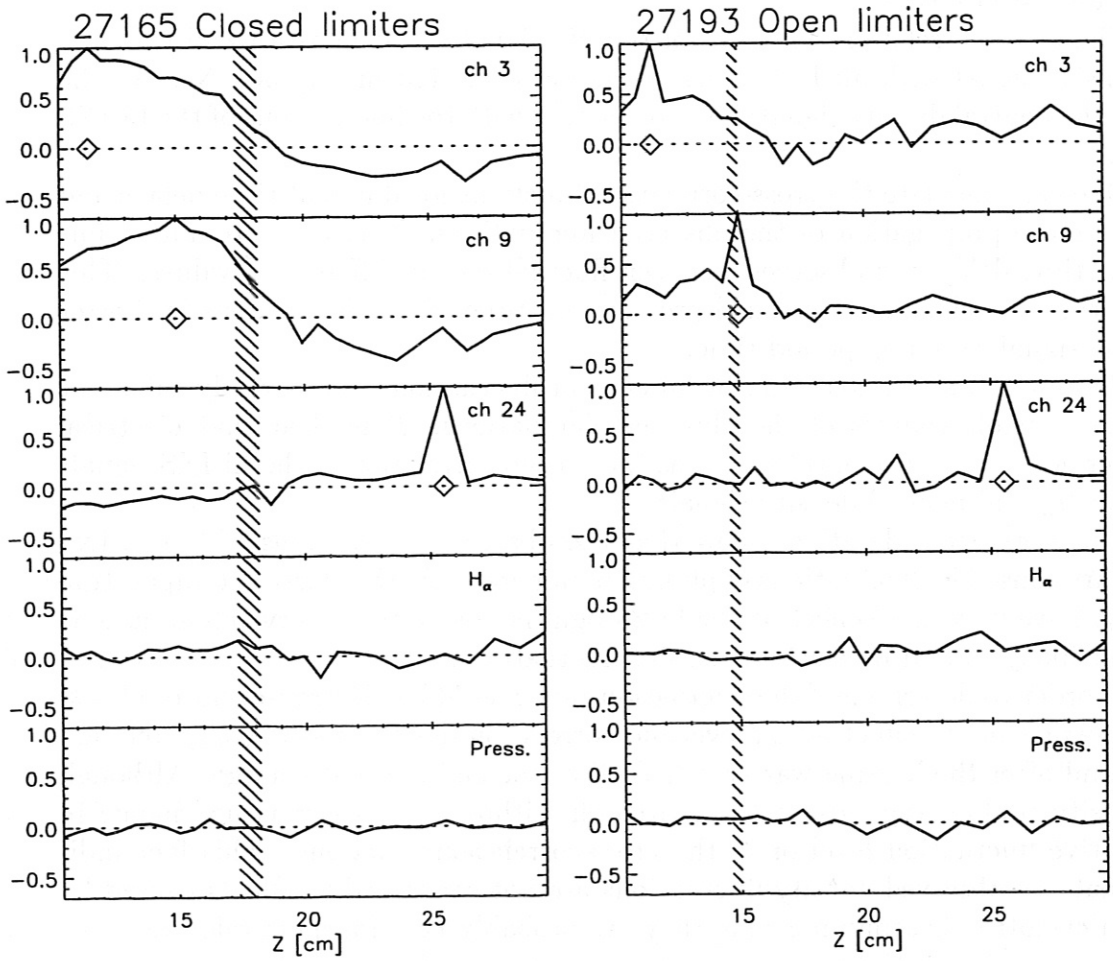

Figure 30: Some cross-correlation functions for shots with closed and open limiters. ($B_0 = 1.27T, \iota(a) = 0.345$) Upper three curves plot $C(Z_1, Z_2)$ against Z_2 for three different Z_1 values. The value Z_1 is indicated in these figures with a diamond. The lower two curves plot the cross-correlation of the H_α signal and the neutral density signal (Press.) with the Li-IXS signals.

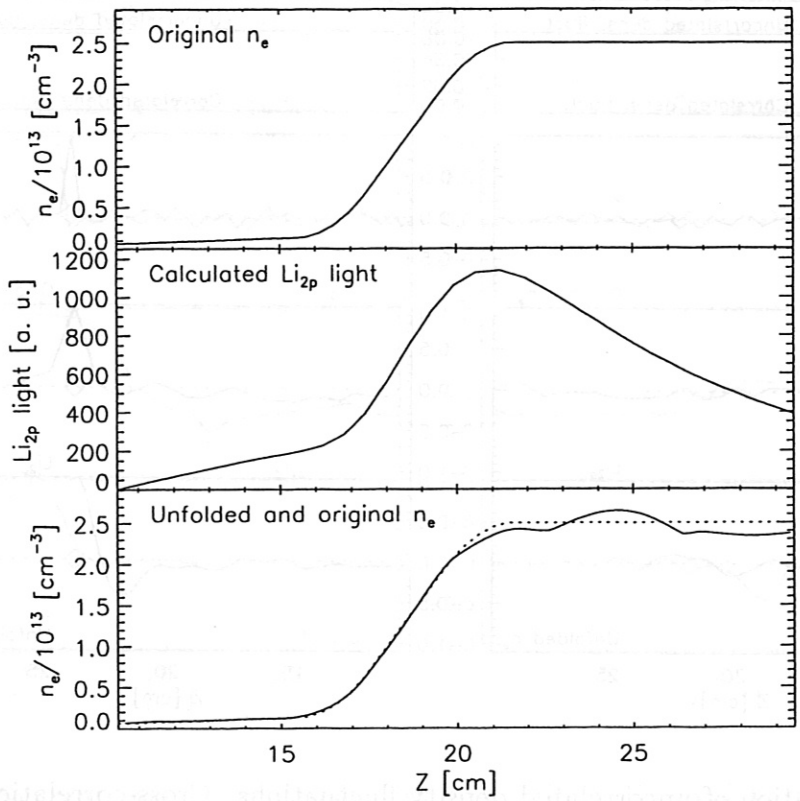

Figure 31: Original density profile, calculated Li 2p light profile and reconstructed density from the computer simulation.

bution at each time point, and look for cross-correlations in the time evolution of the electron density at different places. Although this would be the correct procedure, one has to keep in mind that the electron density at a given place is calculated by taking into account the whole Li 2p light profile, both outside and inside the point in question. In this way fluctuations in the Li 2p light at a single Li-IXS signal (e.g. photon statistical noise, amplifier noise, etc.) cause fluctuations in the whole calculated electron density profile. This mechanism might generate spatially correlated fluctuations in the reconstructed electron density profile without any correlation in the real electron density fluctuations.

In order to investigate the effect of the above processes, detailed numerical simulations were done using realistic density profiles and fluctuation sources. First a base electron density distribution was selected. The time evolution of a test electron density profile was determined by adding computer generated fluctuations to the base distribution. Li 2p light profiles were calculated from each time slice of this

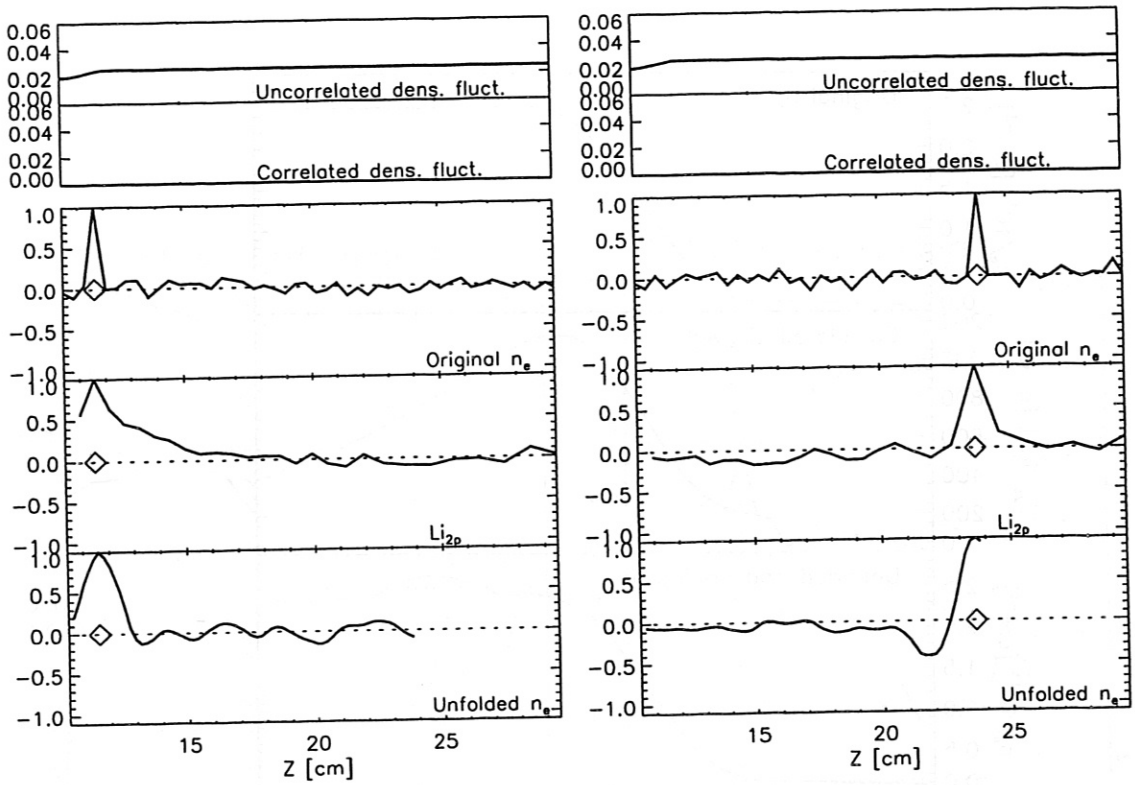

Figure 32: Simulation of uncorrelated density fluctuations. Cross-correlation functions relative to $Z = 12cm$ (left) and $Z = 24cm$ (right) for the original density, Li 2p light and unfolded electron density. The base density distribution is the same as shown in Fig. 31. The fluctuation amplitudes are plotted in $10^{13}cm^{-3}$ units. For more explanation cf. text.

two-dimensional (space-time) test electron density distribution. After adding some computer generated noise to the Li 2p light profiles, the density distribution at each time point was calculated independently. Two-dimensional cross-correlation functions $C(Z_1, Z_2)$ at zero time delay of the fluctuations were calculated for the original electron density, the Li 2p light and the unfolded electron density distributions.

The time averaged original density profile, the calculated Li 2p light profile and unfolded electron density profile is shown in Fig. 31. Cross-correlation functions relative to two positions are shown in Fig. 32 for the case, when spatially uncorrelated density fluctuations were added to the base density distribution. The amplitude distribution of both the correlated and uncorrelated density fluctuations are plotted in $10^{13}cm^{-3}$ units. The fluctuation amplitude had a normal probability distribution and no temporal correlation. The fluctuations added to the light profile were 2% at the maximum of the Li 2p light profile and changed with the square root of the signal. This noise source was added to simulate both photon statistical and

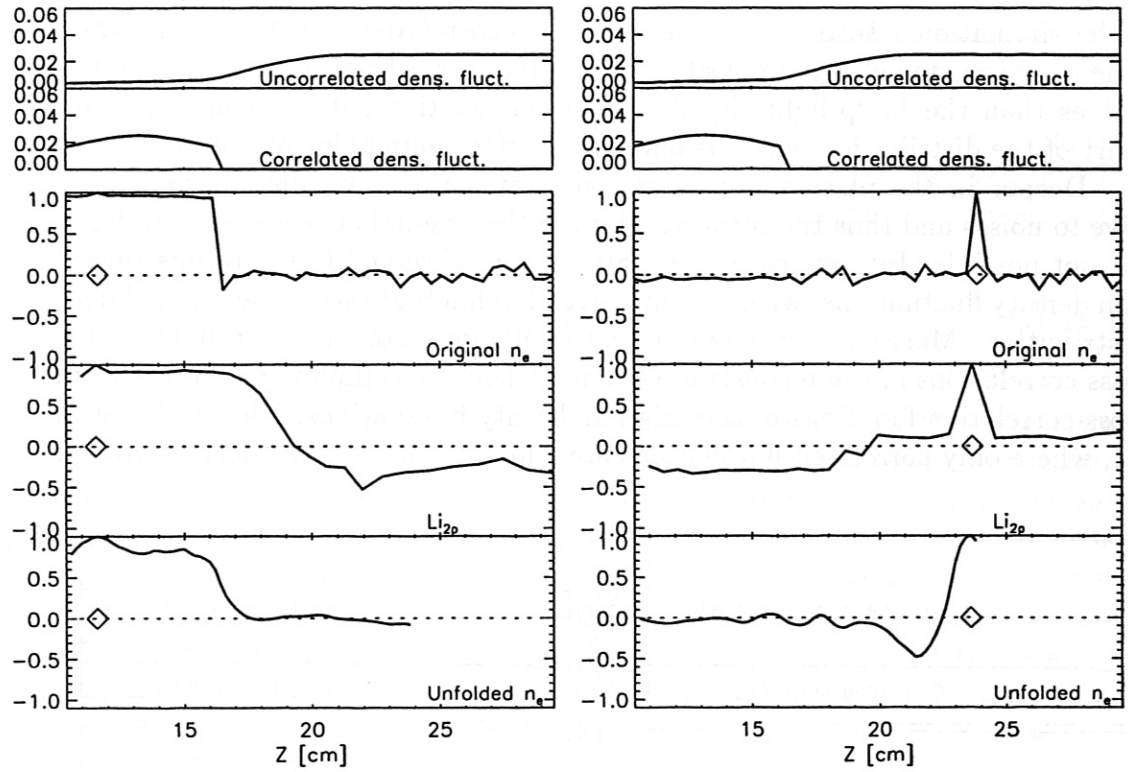

Figure 33: Simulation of correlated density fluctuations. For explanation see caption of Fig. 32.

electronic measurement noises. One can clearly see the cross-correlation of the Li 2p light signal fluctuations introduced by the lifetime of the Li 2p level. The cross correlation functions of the reconstructed electron density are closer to the cross correlations of the original electron density than the ones in the light signals. However, in many cases additional correlated density fluctuations are introduced by the reconstruction algorithm especially at positions where Li-beam attenuation is important.

Fig. 33 shows cross-correlation functions when uncorrelated density fluctuations at the plasma edge were replaced by spatially correlated ones. The most striking effect on the cross-correlation functions of the Li 2p light profile is the appearance of a high negative correlation between the edge and the plasma core, as shown in the left-middle curve of Fig. 33. This negative correlation is caused by Li-beam attenuation. When the fluctuations increase the density at the edge, the beam becomes increasingly attenuated, and as a consequence the Li 2p light intensity drops in the plasma core. Such negative correlation is sometimes present for measured fluctuations (see. Fig. 30), but its amplitude never reaches similar high values as in the simulation.

The simulation results show, that the cross-correlation functions calculated from the reconstructed electron density profiles give correlation lengths closer to the real values than the Li 2p light signal correlation functions, if one considers only that part of the distribution which is outside the maximum point of the Li 2p light profile. Deeper in the plasma the density reconstruction procedure becomes too sensitive to noises and thus the reconstruction of the original cross-correlation functions is not possible. In some cases correlations were observed in the reconstructed electron density fluctuations, without any correlated fluctuations of the original density distribution. Moreover, close and after the maximum of the Li 2p light profile the cross correlations in the reconstructed density become completely different from the cross-correlation functions of the original density fluctuations. This is shown in Fig. 34, where only correlated fluctuations are added to the original density profile.

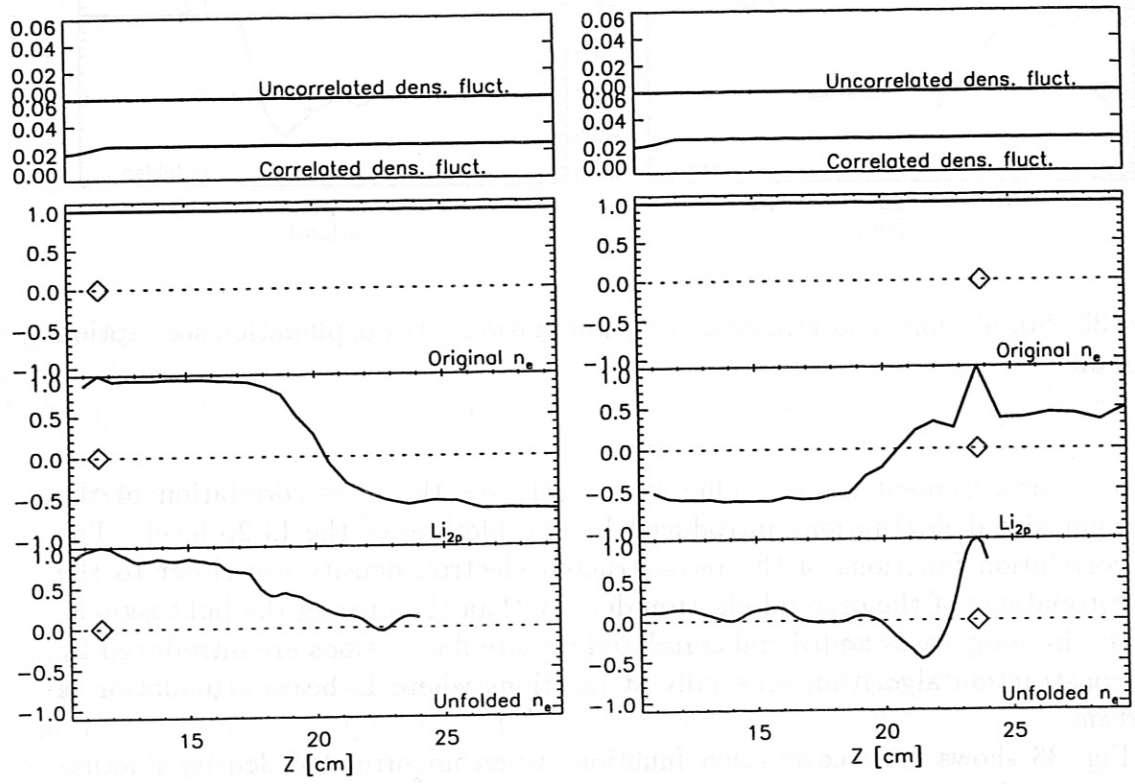

Figure 34: Simulation of density fluctuations correlated accross the whole observed plasma volume. For explanation see caption of Fig. 32.

On the other hand, beam attenuation and the lifetime of the Li 2p atomic level introduces correlations between Li 2p light fluctuations at different Z coordinates, even for the case of uncorrelated density fluctuations. This makes the interpretation of cross-correlation functions more difficult. Despite these problems, one can formu-

late two statements based on the cross-correlation of measured Li 2p light signals for the given experimental configuration and fluctuation level:

- The measured correlation length in the SOL (see Fig. 30) is longer than the one introduced by the lifetime of the Li 2p atomic level (see Fig. 32), thus the SOL density fluctuations seem to have a correlation length comparable to the SOL thickness.

- Using the present evaluation method it is not possible to resolve the correlation of density fluctuations close to and behind the peak of the Li 2p light profile.

The origin of the density fluctuations is not yet clear, but they are always observed [16]. A modulation of the gas inlet rate at the gas valve of the stellarator might be a possible explanation, but several considerations are in contradiction to this hypothesis. If the gas flux fluctuates, one should observe this on the H_α signal, but there is definitely no correlated modulation there. If the gas valve produce such fast pressure fluctuations in the vacuum chamber, it should be observed by the neutral density measurement of the Li-beam diagnostic, which is not the case.

Acknowledgements

Two of the authors (S.Z. and G.K.) would like to thank for the hospitality and support of IPP and especially of the W7–AS Team. One of the authors (S.F.) was financially supported by a project, headed by Prof. HP. Winter, of the Friedrich Schiedel Stiftung für Energieforschung.

References

[1] J. Sapper and H. Renner, *Fusion Technol.* **17** 62 (1990)

[2] K. McCormick, S. Fiedler, G. Kocsis, *et al.*, *IPP-Report*, IPPIII/211 (1996)

[3] K. McCormick, S. Fiedler, P. Platzer, *et al.*, *21th EPS Conference on Plasma Physics and Contr. Fusion, 1994, Montpellier*, p. III–1268

[4] J. Kisslinger, H. Wobig, *12th European Conf. on Controlled Fusion and Plasma Physics, Budapest*, 1985, p. I–453

[5] J. Schweinzer, E. Wolfrum, F. Aumayr, *et al.* , *Plasma Physics and Contr. Fus.* **34** 1173 (1992)

[6] S. Fiedler, K. McCormick, J. Schweinzer, *et al.*, *21th EPS Conference on Plasma Physics and Contr. Fusion, 1994, Montpellier*, p. III–1272

[7] V. Erckmann, F. Wagner, J. Baldzuhn, *et al.*, *Phys. Rev. Lett.* **70** 2086 (1993)

[8] H. Zohm, *Plasma Physics and Controlled Fusion* **38** 105 (1996)

[9] C. Gourdon, D. Marty, E.K. Maschke and J.P. Dumont, *Plasma Phys. and Contr. Nucl. Fus. Res.* **I** 847 (1969)

[10] F.Rau, J. Kisslinger, H. Wobig, *IPP-Report*, IPP 2/259 (1982)

[11] R. Jaenicke, E. Ascasibar, P. Grigull, *et al. Nuclear Fusion* **33** 687 (1993)

[12] F. Wagner and K. Lackner in *Proceedings of the NATO advanced study institute* (New York, Plenum Press, 1986, eds. D.E. Post, R. Behrisch)
and B. LaBombard, MIT Plasma Fusion Center Report No. PFC/RR–86–6 (1986)

[13] G.K. McCormick, Z.A. Pietrzyk, the ASDEX Team and the NI Team, *J. Nucl. Mat.* **162-164** 264 (1989)

[14] Y. Feng, P. Grigull, F. Sardei, *et al.*, 22nd EPS Conference on Plasma Phys. and Contr. Fusion, 1995, Bournemouth, p. IV–325

[15] J. Das, P. Grigull, G. Herre, J.V. Hoffmann, *et al.* F. Sardei, 22nd EPS Conference on Plasma Phys. and Contr. Fusion, 1995, Bournemouth, p. IV–313

[16] M. Endler, L. Giannone, K. McCormick, *et al.*, *Physica Scripta* **51** 610 (1995)